Pure Appl. Chem., Vol. 76, No. 12, pp. 2147–2180, 2004.

INTERNATIONAL UNION OF PURE AND APPLIED CHEMISTRY

PHYSICAL AND BIOPHYSICAL CHEMISTRY DIVISION*

ELECTROCHEMISTRY AT THE INTERFACE BETWEEN TWO IMMISCIBLE ELECTROLYTE SOLUTIONS

(IUPAC Technical Report)

Prepared for publication by
ZDENĚK SAMEC

J. Heyrovský Institute of Physical Chemistry, Academy of Sciences of the Czech Republic, Dolejškova 3, 182 23 Prague 8, Czech Republic

*Membership of the Physical and Biophysical Chemistry Division during the preparation of this report was as follows:

***President*:** R. D. Weir (Canada, 2004–2005); ***Past-President*:** J. Ralston (Australia, 2002–2003); ***Secretary*:** M. J. Rossi (Switzerland, 2000–2005); ***Titular Members*:** G. H. Atkinson (USA, 2002–2005); W. Baumeister (Germany, 2004–2007); R. Fernandez-Prini (Argentina, 2002–2005); J. G. Frey (UK, 2000–2005); R. M. Lynden-Bell (UK, 2002–2005); J. Maier (Germany, 2002–2005); Z.-Q. Tin (China, 2004–2007); ***Associate Members*:** S. Califano (Italy, 2002–2005); S. Cabral de Menezes (Brazil, 2004–2005); A. J. McQuillan (New Zealand, 2004–2005); D. Platikanov (Bulgaria, 2004–2005); C. A. Royer (France, 2004–2007).

Electrochemistry at the interface between two immiscible electrolyte solutions

(IUPAC Technical Report)

Abstract: This document provides an inventory of theoretical and methodological concepts in electrochemistry at the interface between two immiscible electrolyte solutions (ITIES). Definitions of basic relationships are given, together with recommendations for the preferred symbols, terminology, and nomenclature. Methods of study of ITIES are briefly described, current experimental problems are indicated, and representative experimental data are shown. The practical applications of electrochemistry at ITIES are summarized.

CONTENTS

© 2004 IUPAC, *Pure and Applied Chemistry* 76, 2147–2180

1. SCOPE

An interface between two immiscible electrolyte solutions (ITIES) is formed between two liquid solvents of a low (ideally zero) mutual miscibility, each containing an electrolyte. One of these solvents is usually water, and the other one is a polar organic solvent of a moderate or high dielectric permittivity, such as nitrobenzene or 1,2-dichloroethane, which allows for at least partial dissociation of dissolved electrolyte(s) into ions. Processes taking place at the interface of a low permittivity dielectric (e.g., liquid hydrocarbon) and an aqueous electrolyte solution are beyond the scope of this document.

Electrochemical processes at ITIES have attracted a great deal of interest for two reasons. First, the biomimetic features of these processes have been a concern for over one century [1]. Second, the electrochemical reaction at ITIES represents an essential aspect of various practical applications in chemistry including electroanalysis, phase-transfer catalysis, ion extraction, and electrocatalysis. Ion partition equilibria at ITIES were first studied by Nernst [1]. Nernst's approach to the interfacial potential was further developed by Beutner [2–4], whereas Baur [5,6] attempted to treat it as an adsorption potential. The solution of this problem was worked out by Dean [7] and by Bonhoeffer et al. [8]. Karpfen and Randles [9] introduced the concept of the distribution potential related to the equilibrium partition of an electrolyte. Present understanding of the structure of the ITIES stems in part from the earliest theoretical model by Verwey and Niessen [10], which refers to the classical theory of Gouy [11] and Chapman [12]. Nernst and Riesenfeld [13] were the first to investigate the effect of electric current flow across ITIES on electrolyte depletion and accumulation, which was related to the difference in the transport number of the cation in each phase. The change of the interfacial tension of ITIES during current flow, as observed first by Guastalla [14,15] and ascribed to the phenomenon of electrosorption, was correctly explained by Blank [16] on the basis of the depletion–accumulation effect [13] of surface active electrolytes. After two key contributions, one an experimental method for realizing a polarizable ITIES by Gavach [17], and the other the concept of the ideally polarized ITIES by Koryta [18], this field has grown to become a new branch of electrochemistry. This development has been the subject of numerous reviews [19–30] and monographs [31–34].

The purpose of this document is to provide an inventory of basic theoretical and methodological concepts in electrochemistry at ITIES. In the first part, definitions of basic relationships are given, together with recommendations for the preferred symbols, terminology, and nomenclature. In the second part, methods of study of ITIES are briefly described, current experimental problems are indicated and representative experimental data are shown. In the last part, the practical applications of electrochemistry at ITIES are summarized.

2. DEFINITION OF BASIC RELATIONSHIPS

2.1 Two-phase ionic and electronic equilibria

At the ITIES, there are in principle two types of charge-transfer processes:

a) transfer of an ion $X_i^{z_i}$ with charge number z_i between the aqueous phase w and the organic solvent phase o,

$$X_i^{z_i}(\mathrm{w}) \rightleftharpoons X_i^{z_i}(\mathrm{o}) \tag{1}$$

which describes also the transfer of the electrically neutral species ($z_i = 0$), and

b) electron transfer between a redox couple O1/R1 in the phase w and a redox couple O2/R2 in the phase o, which can be described as

$$O1^{z_{O1}}(w) + R2^{z_{R2}}(o) \rightleftharpoons R1^{z_{R1}}(w) + O2^{z_{O2}}(o) \quad (2)$$

Besides this, each of the heterogeneous charge-transfer reactions 1 and 2 can be coupled to a homogeneous chemical reaction, e.g., electron transfer, in the phase w or o. Often, an ion association or complex formation occurs,

$$X_i^{z_i}(s) + X_j^{z_j}(s) \rightleftharpoons X_iX_j^{z_{ij}}(s) \quad (3)$$

where $z_{ij} = z_i + z_j$ and s = w or o, with the corresponding equilibrium constant K_{ij}(s),

$$K_{ij}(s) = \frac{a_{ij}(s)}{a_i(s)a_j(s)} \quad (4)$$

where a's are the activities of the species involved. A coupling of the ion transfer (eq. 1) with the ion association or complex formation (eq. 3) is denoted as an assisted (or facilitated) ion transfer.

In addition to the charge-transfer reactions described by eqs. 1 and 2, the transfer of both water and organic solvent (S) can occur,

$$S(w) \rightleftharpoons S(o) \quad (5)$$

2.2 Equivalent two-phase Nernst relationship

A particular component of a given phase can be characterized in terms of its content and ability to partake in various processes (chemical reactions, transport processes) using the partial molar Gibbs energy (chemical potential). For an electrically charged phase, this quantity is termed the electrochemical potential of the *i*th component

$$\tilde{\mu}_i(s) = \mu_i^o + RT \ln a_i(s) + z_i F\phi(s) \quad (6)$$

where μ_i^o is the standard chemical potential and ϕ is the inner (Galvani) potential of the phase s. The third term in eq. 6 is a part of the standard chemical potential of the *i*th component, i.e., μ_i^o is the standard chemical potential at $\phi(s) = 0$.

At a constant temperature T and pressure p, the condition of ion-transfer equilibrium 1 is given by

$$\tilde{\mu}_i(w) = \tilde{\mu}_i(o) \quad (7)$$

This condition together with eq. 6 yields the Nernst equation [1] for the difference between the inner (Galvani) potentials of the phases w and o, $\Delta_o^w\phi$,

$$\Delta_o^w\phi = \phi(w) - \phi(o) = \Delta_o^w\phi_i^o + \frac{RT}{z_iF}\ln\frac{a_i(o)}{a_i(w)} \quad (8)$$

The standard Galvani potential difference of ion transfer (or standard ion-transfer potential), $\Delta_o^w\phi_i^o$, is defined by the equation

$$\Delta_o^w\phi_i^o = \frac{\Delta_w^o G_i^o}{z_iF} = \frac{\mu_i^o(o) - \mu_i^o(w)}{z_iF} \quad (9)$$

where $\Delta_w^o G_i^o$ is the standard molar Gibbs energy of ion transfer from phase w to phase o, which is given by the difference in the standard molar Gibbs energy of ion solvation in the two phases. Ions with a large positive or large negative $\Delta_w^o G_i^o$ are denoted as hydrophilic or hydrophobic ions, respectively. The ratio of the ion activities or the ion concentrations in the two phases is the ion partition coefficient P_i or the apparent ion partition coefficient P_i', respectively

$$P_i = \frac{a_i(\mathrm{o})}{a_i(\mathrm{w})} = \exp[\frac{z_i F(\Delta_\mathrm{o}^\mathrm{w}\phi - \Delta_\mathrm{o}^\mathrm{w}\phi_i^\mathrm{o})}{RT}] \tag{10}$$

$$P_\mathrm{i}' = \frac{c_\mathrm{i}(\mathrm{o})}{c_\mathrm{i}(\mathrm{w})} = \exp[\frac{z_\mathrm{i} F(\Delta_\mathrm{o}^\mathrm{w}\phi - \Delta_\mathrm{o}^\mathrm{w}\phi_\mathrm{i}^{\mathrm{o}\prime})}{RT}] \tag{11}$$

The formal Galvani potential difference (or formal ion-transfer potential), $\Delta_\mathrm{o}^\mathrm{w}\phi_i^{\mathrm{o}'}$, is defined as

$$\Delta_\mathrm{o}^\mathrm{w}\phi_i^{\mathrm{o}\prime} = \Delta_\mathrm{o}^\mathrm{w}\phi_i^\mathrm{o} + \frac{RT}{z_i F}\ln\frac{\gamma_i(\mathrm{o})}{\gamma_i(\mathrm{w})} \tag{12}$$

where γ_i's represent the activity coefficients of ion i on an amount concentration basis.

For a neutral particle, $z_i = 0$, eq. 10 reduces to

$$P_i = \frac{a_i(\mathrm{o})}{a_i(\mathrm{w})} = \exp(-\frac{\Delta_\mathrm{w}^\mathrm{o} G_i^\mathrm{o}}{RT}) \tag{13}$$

A similar procedure is applicable to the electron-transfer equilibria, eq. 2, starting with the equilibrium condition [35],

$$\tilde{\mu}_{\mathrm{O1}}(\mathrm{w}) + \tilde{\mu}_{\mathrm{R2}}(\mathrm{o}) = \tilde{\mu}_{\mathrm{R1}}(\mathrm{w}) + \tilde{\mu}_{\mathrm{O2}}(\mathrm{o}) \tag{14}$$

which yields the expression for the equilibrium potential difference

$$\Delta_\mathrm{o}^\mathrm{w}\phi = \Delta_\mathrm{o}^\mathrm{w}\phi_\mathrm{el}^\mathrm{o} + \frac{RT}{F}\ln\frac{a_{\mathrm{O2}}(\mathrm{o})a_{\mathrm{R1}}(\mathrm{w})}{a_{\mathrm{R2}}(\mathrm{o})a_{\mathrm{O1}}(\mathrm{w})} \tag{15}$$

The standard Galvani potential difference of electron transfer (or standard electron-transfer potential), $\Delta_\mathrm{o}^\mathrm{w}\phi_\mathrm{el}^\mathrm{o}$, is related to the standard Gibbs energy of electron transfer from the phase o to the phase w, $\Delta_\mathrm{o}^\mathrm{w}G_\mathrm{el}^\mathrm{o}$,

$$\Delta_\mathrm{o}^\mathrm{w}\phi_\mathrm{el}^\mathrm{o} = \frac{\Delta_\mathrm{o}^\mathrm{w}G_\mathrm{el}^\mathrm{o}}{F} = \frac{\mu_{\mathrm{R1}}^\mathrm{o}(\mathrm{w}) - \mu_{\mathrm{O1}}^\mathrm{o}(\mathrm{w}) + \mu_{\mathrm{O2}}^\mathrm{o}(\mathrm{o}) - \mu_{\mathrm{R2}}^\mathrm{o}(\mathrm{o})}{F} \tag{16}$$

The standard Galvani potential difference $\Delta_\mathrm{o}^\mathrm{w}\phi_\mathrm{el}^\mathrm{o}$ can be further related to the standard electrode potentials $E_{\mathrm{O1/R1}}^\mathrm{o}$ (w) and $E_{\mathrm{O2/R2}}^\mathrm{o}$ (o) corresponding to the electrochemical cell reactions

$$\mathrm{O1}^{z_{\mathrm{O1}}}(\mathrm{w}) + (1/2)\mathrm{H}_2(\mathrm{g}) = \mathrm{R1}^{z_{\mathrm{R1}}}(\mathrm{w}) + \mathrm{H}^+(\mathrm{w}) \tag{17}$$

and

$$\mathrm{O2}^{z_{\mathrm{O2}}}(\mathrm{o}) + (1/2)\mathrm{H}_2(\mathrm{g}) = \mathrm{R2}^{z_{\mathrm{R2}}}(\mathrm{o}) + \mathrm{H}^+(\mathrm{o}) \tag{18}$$

On this basis, eq. 16 can be written in the form [36]

$$\Delta_\mathrm{o}^\mathrm{w}\phi_\mathrm{el}^\mathrm{o} = E_{\mathrm{O2/R2}}^\mathrm{o}(\mathrm{o}) - E_{\mathrm{O1/R1}}^\mathrm{o}(\mathrm{w}) + \Delta_\mathrm{o}^\mathrm{w}\phi_{\mathrm{H}^+}^\mathrm{o} \tag{19}$$

where $\Delta_\mathrm{o}^\mathrm{w}\phi_{\mathrm{H}^+}^\mathrm{o}$ is the standard Galvani potential difference for hydrogen ion transfer.

2.3 Multi-ion partition equilibria

The equilibrium potential difference established in practical liquid–liquid systems is often controlled by the multi-ion partition equilibria rather than by a single ion-transfer reaction. The general theoretical treatment of these systems was given by Hung [37,38] and Kakiuchi [39]. The treatment is based on two general conditions. The first is the electroneutrality condition for N ionic species in each phase, i.e.,

$$\sum_{i=1}^{N} z_i c_i(\mathrm{s}) = 0 \tag{20}$$

The second follows from the mass conservation law, i.e.,

$$\begin{aligned} &c_i(\mathrm{w}) + \sum_{k=1}^{M} \lambda_{ki} c_{ki}(\mathrm{w}) + r[c_i(\mathrm{o}) + \sum_{k=1}^{M} \lambda_{ki} c_{ki}(\mathrm{o})] = \\ &c_i^0(\mathrm{w}) + \sum_{k=1}^{M} \lambda_{ki} c_{ki}^0(\mathrm{w}) + r[c_i^0(\mathrm{o}) + \sum_{k=1}^{M} \lambda_{ki} c_{ki}^0(\mathrm{o})] \end{aligned} \tag{21}$$

where $r = V(\mathrm{o})/V(\mathrm{w})$ is the ratio of the volume of phase o to that of phase w, c_i (s) and c_i^0 (s) are the equilibrium and initial concentrations of the ion i (i = 1, 2,…, N), c_{ki} (s) and c_{ki}^0 (s) are the equilibrium and initial concentrations of the complex or ion pair k (k = 1, 2,..., M), and λ_{ki} is the chemical amount of i in the complex or the ion pair k [39]. Equation 20, N equations (eq. 21) together with N equations (eq. 10) and 2 M equations (eq. 4) represent $2(N + M) + 1$ equations for $2(N + M)$ concentrations of ions and complexes or ion pairs in both phases and the equilibrium potential difference $\Delta_{\mathrm{o}}^{\mathrm{w}}\phi$, i.e., the distribution potential [9].

The analytical solution of this system of equations can be obtained only in some limiting cases [37–39]. The simplest one is represented by the partition of a single binary electrolyte $B_{\nu+}A_{\nu-}$, which completely dissociates in both phases into ν_+ cations B^{z+} and ν_- anions A^{z-}. In this case, the distribution potential depends neither on the volume ratio r nor explicitly on the electrolyte concentration [37],

$$\Delta_{\mathrm{o}}^{\mathrm{w}}\phi = \frac{z_+ \Delta_{\mathrm{o}}^{\mathrm{w}}\phi_{\mathrm{B}^+}^{\mathrm{o}\,\prime} + |z_-| \Delta_{\mathrm{o}}^{\mathrm{w}}\phi_{\mathrm{A}^-}^{\mathrm{o}\,\prime}}{z_+ + |z_-|} \tag{22}$$

For $N > 2$, the system of equations can be simplified, provided that all ionic species are completely dissociated in both phases. Then, a substitution from eq. 21 into eq. 20 yields [37]

$$\sum_{i=1}^{N} z_i \frac{c_i^0(\mathrm{w}) + r c_i^0(\mathrm{o})}{1 + r P_i'} = 0 \tag{23}$$

A prediction of the distribution potential can be based on the assumption that the volume ratio r = 1 [37,38]. Equation 23 with r = 1 was used to analyze the behavior of two macroscopic systems of practical interest. The first one consists of a hydrophobic electrolyte SY in the organic solvent and a hydrophilic electrolyte RX in water, and the second one consists of a hydrophobic electrolyte SY in the organic solvent and an electrolyte SX with the same cation S^+ in water. Provided that $\Delta_{\mathrm{o}}^{\mathrm{w}}\phi_{\mathrm{S}^+}^{\mathrm{o}}$, $\Delta_{\mathrm{o}}^{\mathrm{w}}\phi_{\mathrm{X}^-}^{\mathrm{o}} << 0 << \Delta_{\mathrm{o}}^{\mathrm{w}}\phi_{\mathrm{R}^+}^{\mathrm{o}}$, $\Delta_{\mathrm{o}}^{\mathrm{w}}\phi_{\mathrm{Y}^-}^{\mathrm{o}}$, the distribution potential for the former system is given by [37]

$$\Delta_{\mathrm{o}}^{\mathrm{w}}\phi \approx \frac{RT}{2F} \ln \frac{c_{\mathrm{RX}}^0 \exp(F\Delta_{\mathrm{o}}^{\mathrm{w}}\phi_{\mathrm{X}^-}^{\mathrm{o}} / RT) + c_{\mathrm{SY}}^0 \exp(F\Delta_{\mathrm{o}}^{\mathrm{w}}\phi_{\mathrm{S}^+}^{\mathrm{o}} / RT)}{c_{\mathrm{RX}}^0 \exp(-F\Delta_{\mathrm{o}}^{\mathrm{w}}\phi_{\mathrm{R}^+}^{\mathrm{o}} / RT) + c_{\mathrm{SY}}^0 \exp(-F\Delta_{\mathrm{o}}^{\mathrm{w}}\phi_{\mathrm{Y}^-}^{\mathrm{o}} / RT)} \tag{24}$$

The distribution potential fulfils the inequality $\Delta_{\mathrm{o}}^{\mathrm{w}}\phi_{\mathrm{S}^+}^{\mathrm{o}}$, $\Delta_{\mathrm{o}}^{\mathrm{w}}\phi_{\mathrm{X}^-}^{\mathrm{o}} << \Delta_{\mathrm{o}}^{\mathrm{w}}\phi << \Delta_{\mathrm{o}}^{\mathrm{w}}\phi_{\mathrm{R}^+}^{\mathrm{o}}$, $\Delta_{\mathrm{o}}^{\mathrm{w}}\phi_{\mathrm{Y}^-}^{\mathrm{o}}$ and, hence $a_{\mathrm{S}^+}(\mathrm{o})/a_{\mathrm{S}^+}(\mathrm{w}) >> 1$, $a_{\mathrm{Y}^-}(\mathrm{o})/a_{\mathrm{Y}^-}(\mathrm{w}) >> 1$, $a_{\mathrm{R}^+}(\mathrm{o})/a_{\mathrm{R}^+}(\mathrm{w}) << 1$, and $a_{\mathrm{X}^-}(\mathrm{o})/a_{\mathrm{X}^-}(\mathrm{w}) << 1$. Under these conditions, no stable distribution potential can be established and the state of the system can be controlled by the externally supplied charge (ideally polarizable interface [18]). In the latter case, the distribution of the common cation S^+ determines the distribution potential, i.e.,

$$\Delta_{\mathrm{o}}^{\mathrm{w}}\phi = \Delta_{\mathrm{o}}^{\mathrm{w}}\phi_{\mathrm{S}^+}^{\mathrm{o}} + \frac{RT}{F} \ln \frac{a_{\mathrm{S}^+}(\mathrm{o})}{a_{\mathrm{S}^+}(\mathrm{w})} \tag{25}$$

provided that $\Delta_o^w\phi_{S^+}^o - \Delta_o^w\phi_{X^-}^o >> 4(c_{SX}^0/c_{SY}^0)(1 + c_{SX}^0/c_{SY}^0)$ [37]. These features are important for the design of electrochemical cells that can be used to study polarization phenomena at the ITIES.

On the other hand, in some systems comprising emulsions, vesicles, and liquid membranes the volume ratio approaches one of the limiting values $r \to 0$ and $r \to \infty$. Equation 23 then simplifies to

$$\sum_{i=1}^{N} [z_i c_i^0(\mathrm{w}) \sum_{j \neq i} P_j'] = 0 \tag{26}$$

and

$$\sum_{i=1}^{N} [z_i c_i^0(\mathrm{o}) \sum_{j \neq i} (1/P_j')] = 0 \tag{27}$$

respectively [39], i.e., the distribution potential is independent of r.

The same procedure is used to predict the distribution potential in systems comprising the complex formation or ion association as described by eq. 3 [37–39], which shifts the ion partition equilibrium in favor of one or the other phase. Owing to the electroneutrality condition (eq. 20), this shift is balanced by the redistribution of other ions. The coupling of ion-transfer (eq. 1) and electron-transfer (eq. 2) reactions represents a specific case [40].

2.4 Scale of Galvani potential differences

For thermodynamic reasons, the Galvani potentials ϕ(w) and ϕ(o) as well as their differences $\Delta_o^w\phi$ are not directly accessible from experiment. Therefore, to construct a scale of Galvani potential differences, a nonthermodynamic hypothesis must be introduced, which allows the evaluation of the standard Gibbs energies of transfer for individual ions and, therefore, the standard ion-transfer potentials according to eq. 9. Experimental data for such an evaluation is provided by partition, solubility, potentiometric, and voltammetric measurements.

The partition equilibrium of a single binary electrolyte $B_{\nu+}A_{\nu-}$, which gives rise to the distribution potential described by eq. 22, can be characterized by the measurable parameter, the partition coefficient P_{BA} given by

$$P_{BA} = \exp[-\frac{\Delta_w^o G_{BA}^o}{(\nu_+ + \nu_-)RT}] = \frac{a_\pm(\mathrm{o})}{a_\pm(\mathrm{w})} = \frac{\gamma_\pm(\mathrm{o})c_{BA}(\mathrm{o})}{\gamma_\pm(\mathrm{w})c_{BA}(\mathrm{w})} \tag{28}$$

where $\Delta_w^o G_{BA}^o$ is the standard Gibbs energy of electrolyte transfer,

$$\Delta_w^o G_{BA}^o = \nu_+ \Delta_w^o G_{B^{z+}}^o + \nu_- \Delta_w^o G_{A^{z-}}^o \tag{29}$$

$a_\pm$ is the mean activity, $\gamma_\pm$ is the mean activity coefficient, and c_{BA} is the electrolyte concentration. The most commonly used nonthermodynamic hypothesis is Parker's assumption [41] that the cation and anion of tetraphenylarsonium tetraphenylborate (Ph_4AsPh_4B) have equal molar standard Gibbs energies of transfer, i.e.,

$$\Delta_w^o G_{Ph_4As^+}^o = \Delta_w^o G_{Ph_4B^-}^o \tag{30}$$

This assumption allows the evaluation of $\Delta_w^o G_{Ph_4As^+}^o$ and $\Delta_w^o G_{Ph_4B^-}^o$ from partition measurements of Ph_4AsPh_4B. Standard Gibbs energies of transfer of other ions are then obtained from the partition measurements of their salts with Ph_4As^+ or Ph_4B^-.

Solubility measurements yield the concentrations c_{BA}^s (w) and c_{BA}^s (o) of the saturated solutions of the electrolyte $B_{\nu+}A_{\nu-}$ in the w and o phases at a given temperature. When the ion association con-

stants are known, the mean activity $a_{\pm}^{s}$ of the electrolytes and the standard Gibbs energies ΔG_{BA}^{o} (w) and ΔG_{BA}^{o} (o) of solution (in the molar scale) can be calculated, e.g., for the phase w [42],

$$\Delta G_{BA}^{o}(w) = -(\nu_{+} + \nu_{-})RT \ln a_{\pm}^{s}(w) \tag{31}$$

The value of the standard Gibbs energy of electrolyte transfer, $\Delta_{w}^{o}G_{BA}^{o}$, is then obtained as the difference

$$\Delta_{w}^{o}G_{BA}^{o} = \Delta G_{BA}^{o}(o) - \Delta G_{BA}^{o}(w) \tag{32}$$

In general, the standard Gibbs energies inferred from partition and solubility measurements differ, because in the former case, the equilibrium partition of both solvents according to eq. 5 takes place, i.e., the two solvents are mutually saturated.

Potentiometric and voltammetric measurements of the standard Gibbs ion-transfer energies are discussed in Section 4.

2.5 Charge-transfer rate constants

2.5.1 Apparent kinetic parameters

Ion-transfer reaction (1) can be described by the first-order rate law

$$J_i = k_f c_i(w) - k_b c_i(o) \tag{33}$$

where J_i is the ion flux from the phase w to the phase o, c_i(w) and c_i(o) are the ion concentrations in the aqueous and the organic solvent side of the ITIES, and k_f and k_b are the heterogeneous rate constants (m s^{-1}) for the forward or backward ion transfer, respectively. The rate constants k_f and k_b are related to each other by virtue of the principle of microscopic reversibility, i.e.,

$$k_f / k_b = \exp(-\Delta_{w}^{o}\tilde{\mu}_i^{o} / RT) = \exp[z_i F(\Delta_{o}^{w}\phi - \Delta_{o}^{w}\phi_i^{o})RT] \tag{34}$$

where $\Delta_{w}^{o}\tilde{\mu}_i^{o}$ is the standard electrochemical Gibbs energy of ion transfer. Equation 33 holds irrespective of the actual dependence of the rate constant on the potential difference $\Delta_{o}^{w}\phi$. For the sake of comparison, two apparent kinetic parameters are introduced. The first is the apparent standard rate constant k_0^s at the standard Galvani potential difference $\Delta_{o}^{w}\phi_i^{o}$,

$$k_0^s = k_f(\Delta_{o}^{w}\phi = \Delta_{o}^{w}\phi_i^{o}) = k_b(\Delta_{o}^{w}\phi = \Delta_{o}^{w}\phi_i^{o}) \tag{35}$$

The second parameter is the apparent charge-transfer coefficient α, which characterizes the potential dependence of the forward rate constant,

$$\alpha = (RT / z_i F)(\partial \ln k_f / \partial \Delta_{o}^{w}\phi) \tag{36}$$

On the other hand, the electron-transfer reaction (eq. 2) is described by the second-order rate law,

$$J_{el} = k_f c_{R1}(w) c_{O2}(o) - k_b c_{O1}(w) c_{R2}(o) \tag{37}$$

where J_{el} is the electron flux from phase w to phase o. The units for the forward and backward heterogeneous rate constants are m^4 mol^{-1} s^{-1}. The relationship between k_f and k_b is analogous to that in eq. 34,

$$k_f / k_b = \exp(-\Delta_{w}^{o}\tilde{\mu}_{el}^{o} / RT) = \exp[-F(\Delta_{o}^{w}\phi - \Delta_{o}^{w}\phi_{el}^{o})RT] \tag{38}$$

where $\Delta_{w}^{o}\tilde{\mu}_{el}^{o}$ is the standard electrochemical Gibbs energy of electron transfer from the phase w to the phase o. As above, two apparent kinetic parameters are introduced, i.e., the apparent standard rate constant k_0^s at the standard Galvani potential difference, $\Delta_{o}^{w}\phi_{el}^{o}$, and the apparent charge-transfer coefficient α,

$$\alpha = -(RT / F)(\partial \ln k_f / \partial \Delta_o^w \phi) \tag{39}$$

2.5.2 Theoretical relationships

Owing to the presence of an electrical double layer at the ITIES, the concentrations of ions participating in the ion (1) or electron (2) transfer reactions depend on the coordinate x perpendicular to the interface. The static double-layer effect is accounted for by assuming an equilibrium ionic distribution up to the positions $x = a$ and $x = b$ located close to the interface in phases w and o, respectively, between which the ion or electron is driven by the local potential gradient to cross the interface. The apparent forward rate constant k_f is then expressed by

$$k_f = k_{ft} \rho(a,b) \tag{40}$$

where k_{ft} is the true rate constant and $\rho(a,b)$ is the probability that the ion in reaction 1 reaches the position $x = a$, or the redox species R1 and O2 in reaction 2 reach the position $x = a$ and $x = b$, respectively.

Theories of elementary ion transfer from a to b are based on the multi-barrier or stochastic models [43–48]. Phenomenologically, the true rate constant can be described by the Butler–Volmer equation [35,43], or by the integral form of the Nernst–Planck equation [44,45],

$$k_{ft} = \frac{D}{\int_a^b \exp[\Delta f(x)]\mathrm{d}x} \tag{41}$$

where D is the local mean diffusion coefficient of the ion, $f(x) = \tilde{\mu}^o(x)/RT$ is the dimensionless standard electrochemical potential, and $\Delta f(x) = f(x) - f(a)$. The dynamic double-layer effect has been also treated theoretically [49,50].

Theoretical approaches to elementary electron transfer [35,51–53] are based on the quantum mechanical [54] or nonequilibrium thermodynamic [55] theory of electron-transfer reactions in polar media. The expression for the true rate constant of electron transfer from a to b has the form

$$k_{ft} = Z \exp(-\Delta G^{\ddagger} / RT) \tag{42}$$

where the pre-exponential factor Z accounts for the non-adiabacity effect [53], $\Delta G^{\ddagger}$ is the Gibbs activation energy,

$$\Delta G^{\ddagger} = \frac{(\lambda + \Delta_a^b \tilde{\mu}_{el}^o)^2}{4\lambda} \tag{43}$$

λ is the sum of the solvent and intramolecular reorganization energies, and $\Delta_a^b \tilde{\mu}_{el}^o$ is the standard electrochemical Gibbs energy of the electron-transfer change from $x = a$ to $x = b$, cf. eq. 38.

2.6 Electric current

The electric current I flowing through an ITIES is related to the one-dimensional ionic fluxes J_i, in the direction from the phase w to the phase o, through the general relationship

$$I / A = \sum_i z_i F J_i \tag{44}$$

where A is the area of the interface. This definition is consistent with the commonly accepted sign of the electric current, which is considered as positive when a net positive charge is transferred from w to o.

3. METHODS OF STUDY

3.1 Polar organic solvents immiscible with water

Polar organic solvents exhibiting very low miscibility with water that have been used in electrochemical studies on ITIES include, e.g., nitrobenzene, nitroethane, *o*-nitrophenyl octyl ether, *o*-nitrotoluene, chloroform, 1,2-dichloroethane, acetophenone, 2-heptanone, 2-octanone, and benzonitrile. Some properties of the most commonly used solvents are given in Table 1.

Table 1 Comparison of some properties of *o*-nitrophenyl octyl ether (*o*-NPOE), nitrobenzene (NB), and 1,2-dichlororethane (DCE) at 298 K: molar mass M, density ρ, molar volume, V_m, effective solvent radius r, shear viscosity η, relative dielectric permittivity ε_r, surface tension σ, solubility of the organic solvent in water, c_s^0 and water in organic solvent c_{aq}^0. Excerpted from [142].

Property	*o*-NPOE	NB	DCE
M/g mol^{-1}	251.33	123.11	98.96
ρ/g cm^{-3}	1.041[a]	1.1984	1.2458
V_m/cm^3 mol^{-1}	241.4	102.7	79.4
r/nm	0.368	0.277	0.254
η/mPa s	13.8	1.795	0.779
ε_r	24.2	34.82	10.36
σ/mN m^{-1}	–	42.76	31.54
c_s^0/mol dm^{-3}	2.01×10^{-6}	1.5×10^{-2}	8.5×10^{-2}
c_{aq}^0/mol dm^{-3}	4.61×10^{-2}	0.2	0.11

[a]293 K

3.2 Measurements of equilibrium potential differences

Research on equilibrium galvanic and voltaic cells comprising an ITIES belongs to the earliest activities in the field of electrochemistry on liquid–liquid interfaces [1], see ref. [56] for review. From a practical point of view, the main difficulty is connected with the reference electrode in the organic phase. To circumvent this problem in a galvanic cell, an aqueous reference electrode is usually used which, however, requires introducing a second ITIES, i.e., schematically

$$\text{RE} \parallel \text{w}' \mid \text{o}' \mid \text{o} \mid \text{w} \parallel \text{RE} \tag{45}$$

where the single vertical bar represents the phase boundary, the double vertical bar represents the liquid junction, in which the liquid junction potential is assumed to be eliminated, REs are conventional aqueous reference electrodes (e.g., saturated calomel or silver-silver chloride electrodes), and w (w') or o (o') represent the aqueous or the organic phases, respectively, containing one or more electrolytes. The equilibrium potential difference E_{cell} of the cell (45) can be written as

$$E_{cell} = E_R - E_L = \Delta_o^w\phi - \Delta_{o'}^{w'}\phi + E_j = \Delta_o^w\phi - E_{ref} \tag{46}$$

where E_R and E_L are the electrode potentials of the reference electrode on the right- and left-hand side, respectively, and E_j is the liquid junction potential at the o|o' interface. The potential difference $\Delta_{o'}^{w'}\phi$ can be fixed by the equilibrium salt [9] or ion [17] partition, cf. eqs. 22 or 25, respectively. A suitable cell for measuring the difference in the distribution potentials of the salts RX and R'X' is represented by the scheme

$$\text{RE} \parallel \text{R'X' (w')} \mid \text{R'X' (o')} \mid \text{RX (o)} \mid \text{RX(w)} \parallel \text{RE} \tag{47}$$

A typical cell design is shown in Fig. 1. Analogously, the cell for measuring the difference between the distribution potentials of two ions, e.g., M^+ and S^+, is represented by the cell

$$\text{RE} \parallel \text{SX(w')} \mid \text{SY(o')} \mid \text{MY + SY (o)} \mid \text{MX + RX (w)} \parallel \text{RE} \tag{48}$$

In the latter case, the standard ion-transfer potentials must fulfil the inequalities $\Delta_o^w\phi_{X^-}^o < \Delta_o^w\phi_{S^+}^o << \Delta_o^w\phi_{M^+}^o << \Delta_o^w\phi_{R^+}^o$, $\Delta_o^w\phi_{Y^-}^o$, cf. Section 3.3. Note that the multiphase system RE ‖ SX(w') | SY(o') can be considered as a reference electrode that is reversible to the cation of the organic phase, i.e., an ion-selective-type electrode. An attempt has been made to design a reference electrode that is reversible to the anion of the organic phase, namely $Ag|AgPh_4B|\ SPh_4B(o)$ electrode [57].

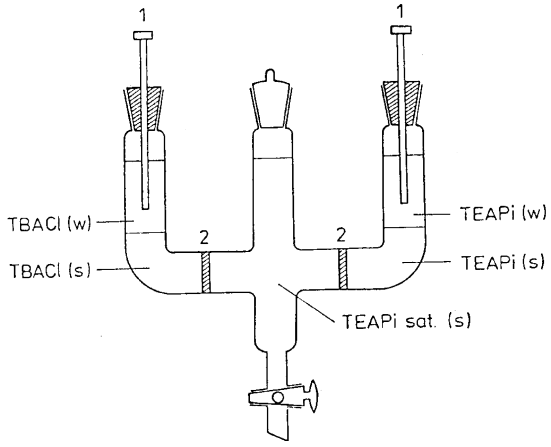

Fig. 1 Scheme of the cell for measuring of the difference between the distribution potentials of tetrabutylammonium chloride (TBACl) and tetraethylammonium picrate (TEAPi): (1) SCE, (2) glass sinters, (w) aqueous phase, (s) organic solvent phase. Reprinted with permission from [56]. © 1987 Springer-Verlag.

In a voltaic cell containing an ITIES, the reference electrode connected to the organic phase is replaced with a metal M, which is separated from the organic phase by an inert gas g [58], cf. Fig. 2 for illustration

$$\text{M} \mid \text{g} \mid \text{o} \mid \text{w} \parallel \text{RE} \mid \text{M'} \tag{49}$$

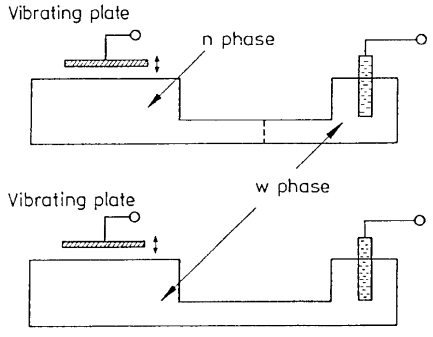

Fig. 2 Schematic illustration of Volta potential measurements by dynamic condenser (Kelvin probe) methods: (w) aqueous phase, (n) organic solvent phase. Reprinted with permission from [56]. © 1987 Springer-Verlag.

By using, e.g., the vibrating electrode (Kelvin probe) method [59], the potential difference E_{cell} of cell (49) is measured under condition such that the outer (Volta) potentials of phases g and o are equal,

$$E_{\text{cell}} = \Delta_{\text{o}}^{\text{w}}\phi + \chi(\text{o}) - E_{\text{ref}} \tag{50}$$

In eq. 50, χ is the surface potential of phase o and E_{ref} comprises contributions that can be considered constant,

$$E_{\text{ref}} = \Phi(\text{M})/F - \delta\chi(\text{M}) - \Delta_{\text{w}}^{\text{M}'}\phi - \mu_{\text{e}}(\text{M}')/F \tag{51}$$

i.e., the electronic work function Φ(M) of the metal M, the change in the surface potential $\delta\chi$(M) of the metal M due to the surface modification if any, and the chemical potential μ_{e}(M') of electrons in the metal contact M' to the reference electrode RE. By comparing the cell potential differences for various partition systems, a scale of distribution potentials can be established, but additional assumptions regarding the contributions of the surface potentials of phases M and o have to be made [56].

3.3 Polarization measurements

3.3.1 Polarizable and nonpolarizable ITIES

An ITIES is classified as being polarizable or nonpolarizable depending on whether a defined relationship exists between the potential difference $\Delta_{\text{o}}^{\text{w}}\phi$ and the concentrations of ions or electrolytes present. Thus, an ITIES where equilibrium partition of a single electrolyte $B_{\nu+}A_{\nu-}$ is established represents a nonpolarizable ITIES, cf. eq. 22, while the equilibrium partition of more than two ions allows for a polarizable ITIES to be formed, cf. eq. 25.

The state of an ideally polarizable ITIES is controlled by the externally supplied charge. Such a system can be realized in the cell

$$\text{RE} \parallel \text{SX(w')} \mid \text{SY(o')} \mid \text{SY (o)} \mid \text{RX (w)} \parallel \text{RE} \tag{48a}$$

provided that the inequalities $\Delta_{\text{o}}^{\text{w}}\phi_{\text{X}^-}^{\text{o}} < \Delta_{\text{o}}^{\text{w}}\phi_{\text{S}^+}^{\text{o}} << 0 << \Delta_{\text{o}}^{\text{w}}\phi_{\text{R}^+}^{\text{o}}, \Delta_{\text{o}}^{\text{w}}\phi_{\text{Y}^-}^{\text{o}}$ are fulfilled [18].

Suitable electrolytes for the aqueous phase w comprise, e.g., LiCl, HCl, $MgCl_2$, $MgSO_4$, while suitable electrolytes for the organic phase o comprise salts of, e.g., tetrabutylammonium, tetraphenylarsonium, or bis(triphenylphosphoranylidene)ammonium cations with tetraphenylborate, tetrakis(4-chlorophenyl)borate, or tetrakis[3,5-bis(trifluoromethyl)phenyl] borate anion. In practice, a small portion of this charge is required to shift the ion and electron partition equilibria in accordance with eqs. 8 and 15. The thermodynamic analysis of the ITIES comprising the bulk (R^+X^-, S^+Y^-) and interfacial (R^+Y^-, S^+X^-) ion pairs yields the electrocapillary equation [60,61]

$$-\text{d}\gamma(T, p = \text{const}) = Q\text{d}E_{\text{o+}}^{\text{w}-} + (\Gamma_{\text{R}^+}^{\text{w,o}} + \Gamma_{\text{RX}}^{\text{w,o}} + \Gamma_{\text{RY}}^{\text{w,o}})\text{d}\mu_{\text{RX}} + (\Gamma_{\text{Y}^-}^{\text{w,o}} + \Gamma_{\text{SY}}^{\text{w,o}} + \Gamma_{\text{RY}}^{\text{w,o}})\text{d}\mu_{\text{SY}} \tag{52}$$

where $\Gamma_i^{\text{w,o}'}$ are relative surface excess concentrations, $E_{\text{o+}}^{\text{w}-}$ is the potential difference of the cell (48a) with the aqueous RE being reversible to anion X^- and the organic RE being reversible to cation S^+. The surface charge density Q,

$$Q = -\left(\frac{\partial\gamma}{\partial E_{\text{o+}}^{\text{w}-}}\right)_{T,p,\mu} = F(\Gamma_{\text{R}^+}^{\text{w,o}} - \Gamma_{X^-}^{\text{w,o}} + \Gamma_{\text{RY}}^{\text{w,o}} - \Gamma_{\text{SX}}^{\text{w,o}}) = F(\Gamma_{\text{Y}^-}^{\text{w,o}} - \Gamma_{\text{S}^+}^{\text{w,o}} + \Gamma_{\text{RY}}^{\text{w,o}} - \Gamma_{\text{SX}}^{\text{w,o}}) \tag{53}$$

sums up the contributions from both the free charge and the charge associated with the adsorption of ion pairs and hence, it represents the total charge density, i.e., the charge that is necessary to supply so as to maintain the state of the interface when the interfacial area is increased by a unit amount [62]. A related quantity is the differential capacity C,

$$C = \left(\frac{\partial Q}{\partial E_{\mathrm{o+}}^{\mathrm{w-}}} \right)_{T,p,\mu} \tag{54}$$

3.3.2 Electrochemical cells

In general, the polarization of an ITIES should be accomplished by means of the four-electrode system [63,64] with two couples of current-supplying (counter) and potential measuring (reference) electrodes, which are connected to phases w and o in the cell (48a). The reference electrodes are usually connected through the Luggin potential probes or capillaries, the tips of which are typically about 1 mm from the boundary. Under some conditions (e.g., low electrical current or large-area reference electrodes), three- [65] or two- [66] electrode configurations are possible, where one or two reference electrodes, respectively, comprise the function of both the reference and counter electrodes.

Electrochemical cells with a planar or spherical liquid–liquid boundary have been in common use. The former cell is illustrated in Fig. 3. The flatness of the boundary and the geometric configuration of the four electrodes are of critical importance for ensuring the homogeneous polarization of the interface. For this reason, the part of the inner space of the cell, which in contact with the organic phase, is often made hydrophobic by treating it with dimethyldichlorosilane [66], or by inserting a piece of plastic tubing [67]. A flat and mechanically stable ITIES can be formed by using an inert thin porous membrane to separate phases w and o [68], or by making one of two immiscible electrolyte solutions a polymer gel [69]. The spherical boundary is encountered in various assemblies with a pendant electrolyte drop [70] or dropping (ascending) [71] electrolyte electrode, cf. Fig. 4 [72]. Micro-sized ITIES (or μITIES) can be realized by supporting ITIES at the tip of a micropipette [73] or on the micro-hole [74] drilled in a polymer film, cf. Fig. 5.

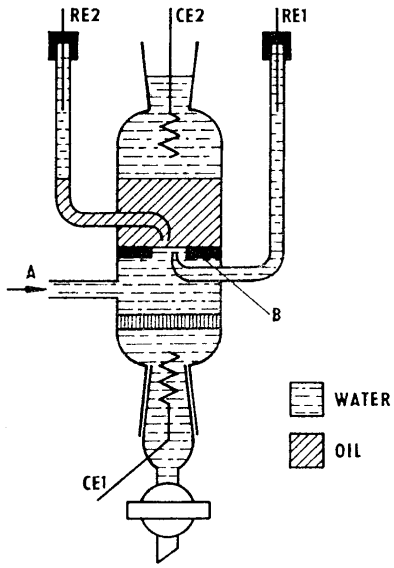

Fig. 3 Scheme of the cell for polarization measurements at a flat ITIES: RE1 (RE2) - reference electrodes, CE1 (CE2) - counter electrodes, A - connection to a microsyringe for the interface adjustment, B - glass barrier with a round hole. Reprinted with permission from [26]. © 1988 Elsevier Science.

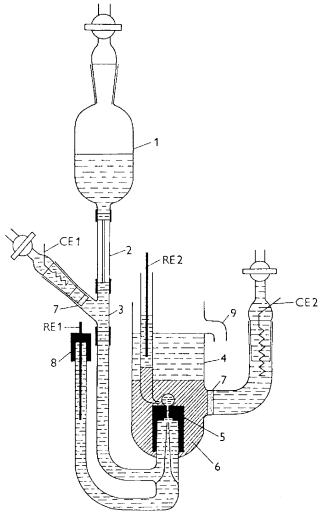

Fig. 4 Scheme of the cell with an electrolyte dropping electrode: 1 - reservoir of aqueous solution, 2 - glass capillary, 3 - column of the aqueous solution, 4 - waste aqueous solution, 5 - PTFE capillary, 6 - organic solvent solution, 7 - sintered glass, 8 - PTFE cap, 9 - outlet to waste, RE1 (RE2) - reference electrodes, CE1 (CE2) - counter electrodes. Reprinted with permission from [26]. © 1988 Elsevier Science.

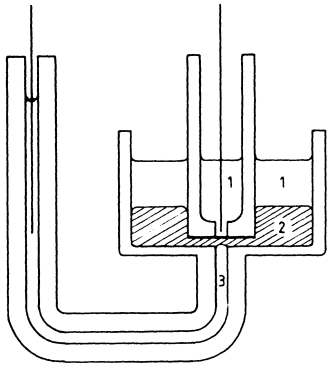

Fig. 5 Scheme of the cell for ITIES at a micro-hole in a thin polymer film: 1 - aqueous electrolyte solution, 2 - organic electrolyte solution, 3 - reference aqueous electrolyte solution for the organic phase. The reference and counter electrodes are Ag|AgCl. Reprinted with permission from [74]. © 1989 Elsevier Science.

Planar liquid–liquid boundaries are encountered also in liquid membrane cells comprising two polarizable ITIES. These cells can be described by the scheme

$$\text{RE} \parallel \text{RX(w')} \mid \text{SY (o)} \mid \text{RX (w)} \parallel \text{RE} \tag{48b}$$

where the current-supplying (counter) electrodes are connected to phases w and w', as schematically shown in Fig. 6. Two types of liquid membranes can be distinguished. Bulk liquid membranes usually consist of a thick layer (1–2 cm) of an organic solvent containing an electrolyte that separates two aqueous electrolyte solutions [75]. Supported liquid membranes (SLMs) have essentially the same configuration, but the organic phase is contained in the pores (0.1–1 μm) of a macroporous polymer sheet the thickness of which is in the range 10–100 μm [76]. An advanced design of SLM with two micro-machined thin polymer films separating the organic and the aqueous phases has been described [77]. Polymer composite liquid membranes represent another modification of SLMs. Thin films (10–100 μm) of the polymer-supported liquid phase are obtained by casting mixtures of a polymer (e.g., PVC)

and the organic solution [78]. The stationary transport can establish on both sides of the SLMs in the rotating diffusion cell [79]. A sketch of such a cell with polarizable SLMs is shown in Fig. 7 [80].

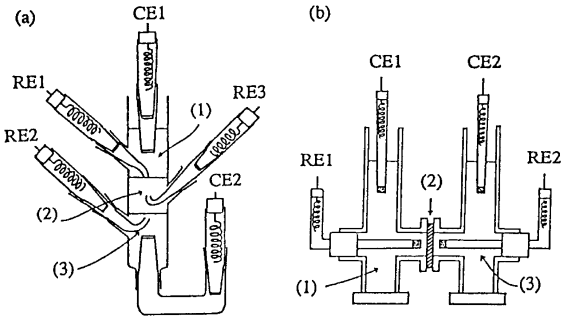

Fig. 6 Scheme of the cells for polarization measurements at bulk liquid (a) and supported liquid (b) membranes: 1,3 - aqueous solutions, 2 - unsupported or supported organic solvent solution, RE1 (RE2, RE3) - reference electrodes, CE1 (CE2) - counter electrodes. Reprinted with permission from [75]. © 1991 The Japan Society for Analytical Chemistry.

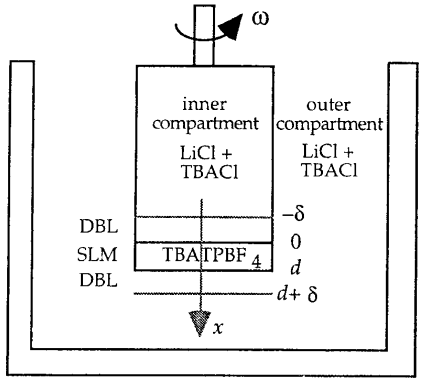

Fig. 7 Scheme of the rotating diffusion cell with a polarizable supported liquid membrane.Reprinted with permission from [80]. © 1998 Elsevier Science.

3.3.3 Polarization methods

The potential difference or the electric current across an ITIES is controlled by means of a potentiostat or galvanostat, respectively. When the current flows through an ITIES, there is always a potential difference between the tips of the Luggin probes and the ITIES due to the solution resistance R, the ohmic potential drop IR, which has to be subtracted from the applied voltage E_{cell},

$$E_{\text{cell}} = \Delta_{\text{o}}^{\text{w}}\phi + IR - E_{\text{ref}} \tag{46a}$$

Once measured (e.g., as the high-frequency limit of the interfacial impedance [81] or the potential step on a galvanostatic transient [82]), the ohmic potential drop can be compensated by means of positive feedback of the potentiostat [64] or by algebraic subtraction under potentiostatic or galvanostatic conditions, respectively. A block scheme of the four-electrode potentiostat is shown in Fig. 8. The potentiostat is driven by the voltage pulse generator (PG), and the current flowing through the cell is measured as the floating voltage drop across the measuring resistor R3. A part of this voltage is fed back to the summing input of the potentiostat for an automatic ohmic drop compensation [64]. A block scheme of a galvanostat is shown in Fig. 9. Current perturbation is generated in the feedback loop of the operational amplifier OA1 by applying a voltage from the voltage PG across the input resistor R. From the

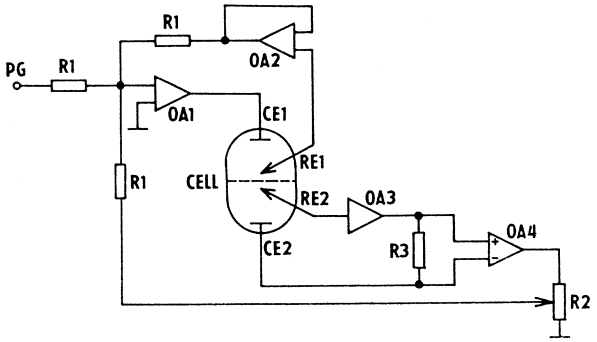

Fig. 8 Block diagram of the four-electrode potentiostat with the positive feedback for ohmic potential drop compensation.

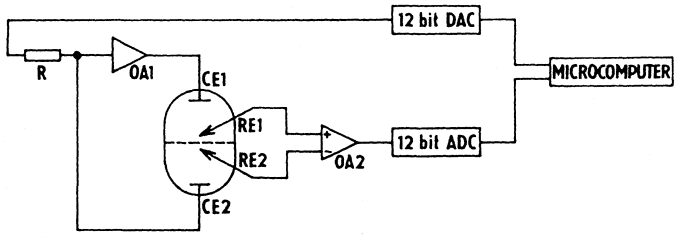

Fig. 9 Block diagram of the electronic circuit for galvanostatic measurements.

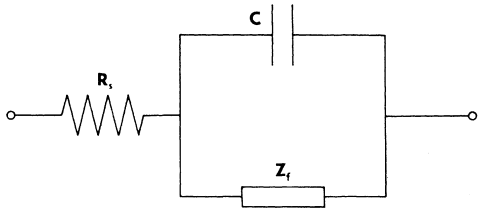

Fig. 10 Randles equivalent circuit for ITIES: C - differential capacity of the interface, Z_f - faradaic impedance, R_s - solution resistance between the tips of Luggin capillaries.

electrical point of view, the ITIES is usually represented by a Randles-type equivalent circuit as shown in Fig. 10.

Both galvanostatic and potentiostatic techniques have been used to study polarization phenomena at the ITIES: current-step chronopotentiometry [63] and chronocoulometry [83], potential-step chronoamperometry [84], cyclic [64] and convolution [85] voltammetry, alternating current voltammetry [81], equilibrium impedance measurements [86], and potential-scan [71] or current-scan [87] polarography with dropping electrolyte electrode. In addition to these techniques, two novel methods have been introduced which do not rely on the electrical perturbation of the ITIES. The first one is based on the analysis of voltage fluctuations resulting from the transfer of ions across an equilibrium ITIES [88], and the other is based on current transient measurements following a step in interfacial area [89]. Discussion of experimental data has been based on the theory of polarography [90] and cyclic voltammetry [91] of electron transfer, on the theory of polarography [92] and cyclic voltammetry of the ion transfer coupled with ion association or complex formation (facilitated ion transfer) [93–97], and on the theory of cyclic voltammetry of ion transfer across a liquid membrane [98,99]. Novel features considered comprise (a) the transport of the electroactive species in the two liquid phases, (b) second-order interfacial electron-transfer reaction, (c) partition (transfer) of the species assisting the simple ion (1) or electron (2) transfer reaction.

The application of various polarization methods has led to (a) evaluation of the differential capacity C of ITIES, eq. 54, from impedance measurements; (b) clarification of the mechanism of various charge-transfer reactions; (c) evaluation of the standard Gibbs energies of ion and electron transfer; (d) determination of the ion diffusion coefficients and the rate constants of the charge-transfer reactions; (e) evaluation of the stoichiometry and the equilibrium constants for coupled complex formation or ion associations, eq. 3.

3.4 Spectroscopic techniques and optical methods

Cyclic voltammetry has been coupled with fluorescence spectroscopy [100] (Fig. 11) or UV–vis absorption spectroscopy [101], the resulting technique being voltfluorometry or voltabsorptometry. In the total internal reflection (TIR) geometry, the absorbance A_{TIR} is given by intergration of the Beer–Lambert law [101]

$$A_{\mathrm{TIR}} = 2\varepsilon \int_0^\infty \frac{c(x,t)}{\cos\theta}\,\mathrm{d}x \tag{55}$$

where θ is the angle of incidence of the light beam at the interface, ε is the molar absorption coefficient of the measured species (e.g., ion or complex) in the phase of higher refractive index, and $c(x,t)$ its concentration at the distance x. A slightly more complicated expression has been derived for the total fluorescence intensity [100]. When voltabsorptometry is used to probe ion transfer (eq. 1), the absorbance is related to the electric current I [101],

$$\frac{\mathrm{d}A_{\mathrm{TIR}}}{\mathrm{d}t} = \frac{2\varepsilon}{z_i FS\cos\theta} I(t) \tag{56}$$

The potential dependence of the time derivative of the absorbance or fluorescence, i.e., the differential cyclic voltabsorptogram or voltfluorogram, has a shape identical to the cyclic voltammogram. A notable advantage of these techniques over cyclic voltammetry is their sensitivity, i.e., a measurable signal can be obtained at much lower concentrations of the transferred ion, which among other factors makes the ohmic drop compensation less significant. Related techniques based on the same principle comprise po-

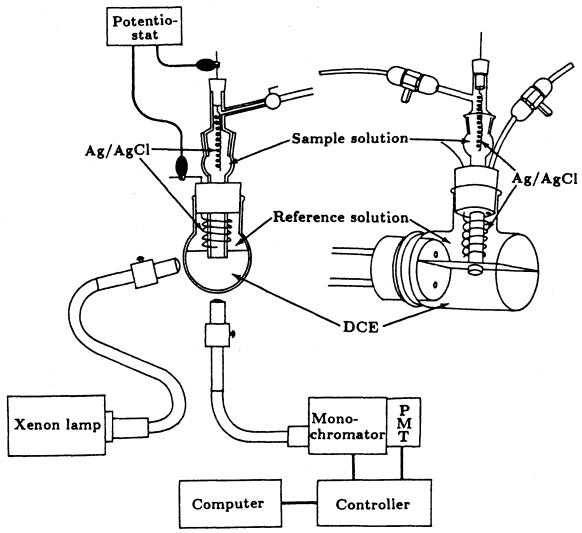

Fig. 11 Scheme of the cell for voltfluorometry. Reprinted with permission from [100]. © 1992 American Chemical Society.

tential step chronofluorometry [102] and chronoabsorptometry [101], and potential modulated reflectance [103]. In the latter case, a small sinusoidal voltage is applied across the ITIES and the in-phase and quadrature components of the reflectance are measured and correlated with the voltage to yield the impedance of the faradaic process [103]. None of these techniques possess ultimate surface specificity because the surface depth resolution is about 100 nm, but they can provide additional information about the mechanism and kinetics of the faradaic process.

On the other hand, it has been established that nonlinear optical methods such as second harmonic generation (SHG) can provide an alternative to study the polarized ITIES with a much more reduced depth resolution [104]. Resolution down to surface monolayer thickness may be reached in the case of SHG, a technique whereby two photons at a fundamental frequency ω are converted into one photon at the harmonic frequency 2ω. Such a surface specificity is obtained due to the lack of centrosymmetry of the interface as compared to the two adjacent bulk solutions. As a result, relative surface coverage, position, and orientation of the adsorbed species with respect to the interface can be monitored [104].

Quasi-elastic laser scattering (QELS) has been introduced as a suitable method for the study of the structure and dynamics of the ITIES, essentially the time-resolved [105] and equilibrium [106] surface tension and visco-elastic properties. Following the simplified description of the method [105], the incident beam normal to the interface is quasi-elastically scattered by the thermally excited capillary wave with a Doppler shift at an angle determined by the ratio of the wavenumbers of the incident beam and the capillary wave (Fig. 12) [105]. The scattered beam is optically mixed with the incident beam at the selected angle by means of a transmission diffraction grating, which yields an optical beat detected at the same frequency as the Doppler shift, i.e., at the capillary wave frequency. Experimentally, the Fourier transform of the power spectrum of the capillary waves is measured and analyzed with the help of the dispersion equation for liquid–liquid interfaces.

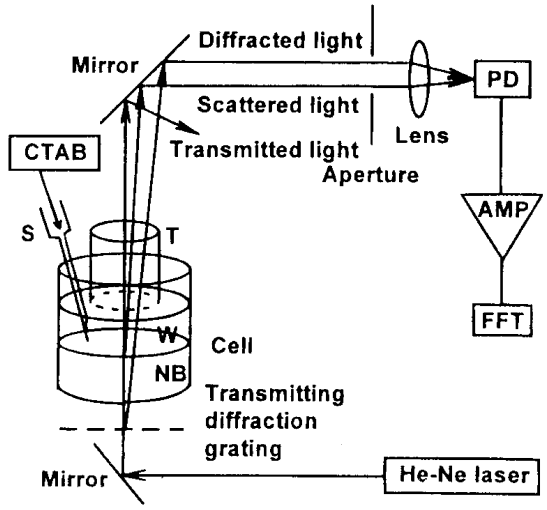

Fig. 12 Scheme of the experimental set up for QELS measurements: w - aqueous solution, NB - organic solvent solution, S - microsyringe, T - glass tube, PD - photodiode, AMP - pre-amplifier, FFT - FFT analyzer. Reprinted with permission from [105]. © 1997 American Chemical Society.

The neutron reflection methodology has been developed for the investigation of the roughness of liquid–liquid interfaces [107]. The experimental design involves establishing a thin (<10 μm) aqueous layer on a single-crystal quartz block, which is then positioned over a PTFE trough containing an organic phase.

The design and operation of the first-ever EPR cell [108] and an ellipsometry apparatus [109] for studying charge-transfer processes at the polarized ITIES have been described.

3.5 Surface tension measurements

The surface tension of nonpolarizable or polarizable ITIES has been measured by classical methods including drop-weight/drop-time, maximum bubble pressure, Wilhelmy plate, Langmuir–Blodgett or pendant-drop method [59]. The latter method has been improved considerably by computer analysis of the video image of the pendant drop (Fig. 13) [110].

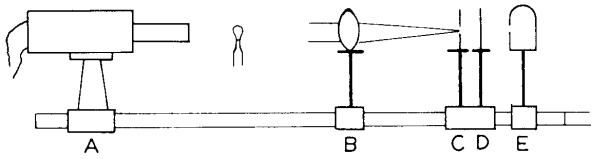

Fig. 13 Scheme of the optical system for video image digitization of the pendant drop: A - video camera, B - biconvex lens, C - iris diaphragm, D - monochromatic green filter, E - light source. Reprinted with permission from [110]. © 1982 Elsevier Science.

3.6 Probing by metal microelectrodes

The application of scanning electrochemical microscopy (SECM) has been extended to studies of electron transfer across the ITIES (Fig. 14) [111]. With SECM, all electrodes are contained in a single phase, and the potential across the ITIES is controlled by the composition of the two liquid phases, essentially by the distribution potential. The rate of electron transfer is determined by measuring the feedback current at a microelectrode. Micro-electrochemical measurement at expanding droplets (MEMED) represents a related method for probing interfacial reactions at the ITIES [112]. Here, the microelectrode is used to measure the local concentration profile of the reactant or the product near the ITIES. The kinetics of the interfacial reaction is evaluated upon modeling mass transport to the expanding droplet.

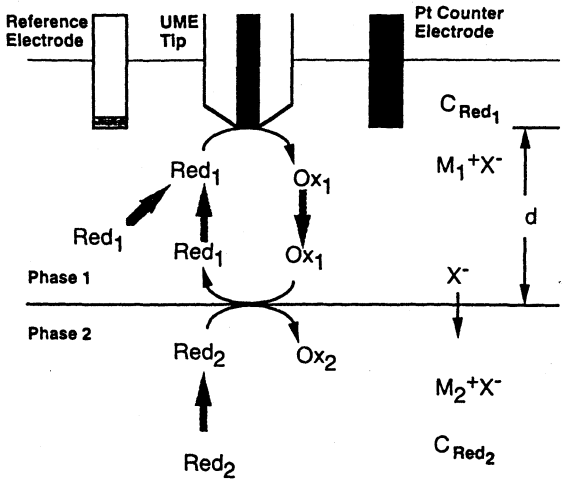

Fig. 14 Schematic diagram of SECM measurements of electron transfer at ITIES: UME – ultra-microelectrode. Reprinted with permission from [111]. © 1995 American Chemical Society.

3.7 Representative experimental data

3.7.1 Simple ion transfer

Figure 15 shows cyclic voltammograms obtained with a planar ITIES using the electrochemical cell [113]

$$\text{Ag} \mid \text{AgCl} \mid \text{SCl(w')} \mid \text{SY (o)} \mid \text{LiCl (w)} \mid \text{AgCl} \mid \text{Ag} \tag{48c}$$

with o = *o*-nitrophenyl octyl ether and SY = tetrabutylammonium tetraphenylborate or tetrapentylammonium tetrakis[3,5-bis(trifluoromethyl) phenyl] borate. Depending on the ion concentrations and the standard ion-transfer potentials $\Delta_o^w\phi_i^o$ (i.e., the standard Gibbs energy of ion transfer $\Delta_w^o G_i^o$), the onset of the electrical current at positive potential differences can be associated with the ion transfer Li^+ (w) → Li^+ (o) and/or Y^- (o) → Y^- (w). Analogously, the onset of the electrical current at negative potential differences can be associated with the ion transfer S^+ (o) → S^+ (w) and/or Cl^- (w) → Cl^- (o). The two current onsets determine the range of the potential differences (so-called potential window), within which the current is associated mainly with the charging of the ITIES. The measured current I is plotted vs. the applied potential E_{cell} after correction for the ohmic potential drop, cf. eq. 46, or vs. the interfacial potential difference $\Delta_o^w\phi$, which is calculated by using eq. 46. A simple method for the voltammetric determination of the zero of the potential scale based on Parker's Ph_4AsPh_4B hypothesis [41] was proposed [114]. When Ph_4AsPh_4B is used as organic supporting electrolyte, and the onsets of the electrical current at positive and negative potential differences are associated respectively with the transfer of Ph_4B^- and Ph_4As^+ ion, the center of symmetry of the current potential curve of the supporting electrolytes should correspond to $\Delta_o^w\phi = 0$ [114]. However, attention must be paid to the salting-out effect, which can lead to an extension of the potential window [115]. The most common procedure for the determination of the reference potential E_{ref} in eq. 46a is based on the voltammetric measurement of a semi-hydrophobic ion transfer of the known standard ion-transfer potential $\Delta_o^w\phi_i^o$. The reference potential is then calculated from the measured reversible half-wave potential $E_{1/2}^{rev}$

$$E_{1/2}^{rev} = \Delta_o^w\phi_i^o + \frac{RT}{z_iF}\ln\frac{\gamma_i(o)}{\gamma_i(w)} + \frac{RT}{2z_iF}\ln\frac{D_i(w)}{D_i(o)} - E_{ref} \tag{57}$$

where the activity coefficient term is estimated by using the Debye–Hückel theory, and the diffusion coefficients are evaluated from voltammetric measurements.

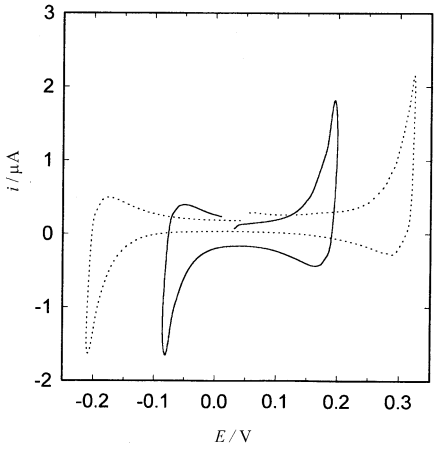

Fig. 15 Cyclic voltammograms of 0.1 M LiCl in water and 0.01 mol dm^{-3} tetrabutylammonium tetraphenylborate (TBATPB) (____) or tetrapentylammonium tetrakis[3,5-bis(trifluoromethyl)-phenyl]borate (TPATFPB) (.....) in *o*-NPOE at sweep rate of 0.02 V s^{-1}, interfacial area 0.14 cm^2. Reprinted with permission from [113]. © 1998 Elsevier Science.

Voltammetric measurements of a simple ion transfer have been used mainly for the determination of ion-transfer potentials and ion-diffusion coefficients. Examples of the cyclic voltammogram and voltfluorogram of a semi-hydrophobic ion transfer are shown in Figs. 16A and 17, respectively.

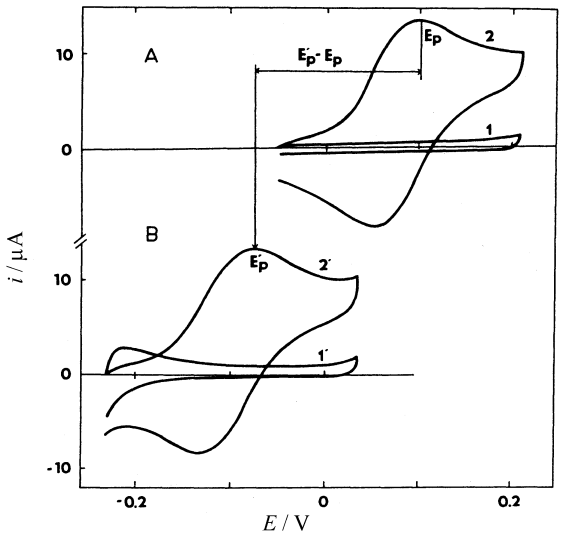

Fig. 16 Cyclic voltammograms of base electrolytes (1, 1') and 1 mmol dm^{-3} 2-phenylethylammonium ion (2, 2') in the absence (A) and presence (B) of 10 mM 2,3,11,12-dibenzo-1,4,7,10,13,16-hexaoxacyclooctadecane (dibenzo-18-crown-6) in the organic phase. Sweep rate 0.02 V s^{-1}. Reprinted with permission from [116]. © 1991 Elsevier Science.

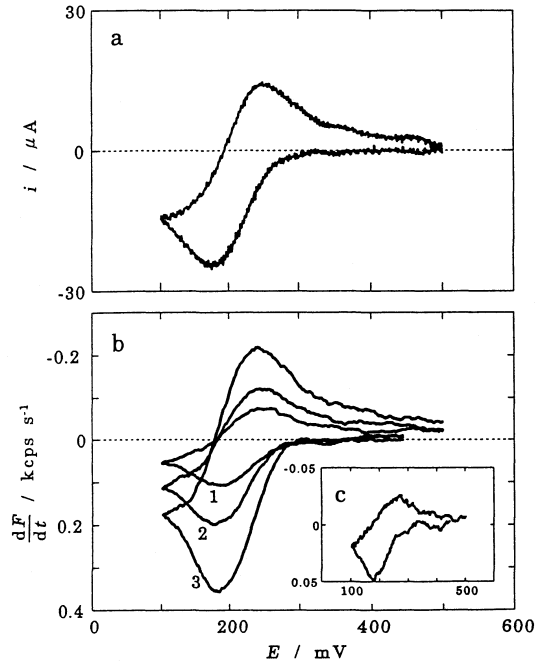

Fig. 17 (a) Cyclic voltammogram of 0.5 mmol dm^{-3} Eosin B in its divalent anionic form (disodium salt of 4',5'-dibromo-2',7'-dinitrofluorescein), and (b) cyclic voltfluorogram at various ion concentrations (nM): 10 (1), 20 (2), 50 (3), or 5 (in set c) at the water - 1,2- dichloroethane interface. Sweep rate 0.2 V s^{-1}. Reprinted with permission from [102]. © 1994 American Chemical Society.

Representative values of the standard ion-transfer potential that are based on voltammetric, partition, and solubility data are listed in Table 2.

Table 2 Standard ion transfer potentials $\Delta_o^w\phi_i^o$ for various water-organic solvent systems from partition (P), solubility (S), and voltammetric (V) measurements.

Ion	$\Delta_o^w\phi_i^o$/V							
	NB			*o*-NPOE		1,2-DCE		
	P[a]	S[b]	V	S[g]	V[g]	P[h]	S[i]	V
H^+	0.337							0.549[j]
Li^+	0.396		0.376[c]					0.591[j]
Na^+	0.354		0.311[c]					0.591[j]
K^+	0.243	0.217	0.222[c]					0.518[j]
Rb^+	0.201	0.199	0.198[c]					0.435[c]
Cs^+	0.160	0.184	0.128[c]	0.238	0.218			0.363[c]
Me_4N^+	0.035	0.041	0.030[d]		0.111	0.182	0.160	0.160[d]
Et_4N^+	–0.059	–0.050	–0.066[d]	0.027		0.044	0.049	0.019[d]
Pr_4N^+		–0.170			–0.090	–0.091	–0.091	
Bu_4N^+	–0.248		–0.275[d]	–0.241		–0.225	–0.182	
Pe_4N^+					–0.324	–0.360		
Hex_4N^+						–0.494		
Ph_4P^+		–0.387					–0.338	
Ph_4As^+	–0.373			–0.314		–0.365	–0.338	
F^-						–0.598		
Cl^-	–0.308	–0.454				–0.481	–0.555	
Br^-		–0.373				–0.398	–0.407	–0.446[k]
I^-	–0.195	–0.227	–0.196[f]			–0.273	–0.261	–0.342[k]
NO_3^-			–0.253[e]			–0.351		
ClO_4^-	–0.083		–0.090[e]	–0.160	–0.136	–0.178	–0.176	–0.170[d]
SCN^-			–0.166[f]			–0.264		
$Picrate^-$	0.048	0.035	0.038[d]					–0.057[d]
Ph_4B^-	0.373			0.314		0.365	0.338	

[a]J. Rais. *Collect. Czech. Chem. Commun*. **36**, 3253 (1970).
[b]A. F. Danil de Namor and T. Hill. *J. Chem. Soc., Faraday Trans. 1* **79**, 2713 (1983).
[c]Z. Samec, V. Mareček, M. P. Colombini. *J. Electroanal. Chem*. **257**,147 (1987).
[d]T. Wandlowski, V. Marecek, Z. Samec. *Electrochim. Acta* **35**, 1173 (1990).
[e]B. Hundhammer, T. Solomon, H. Alemu. *J. Electroanal. Chem*. **149**, 179 (1983).
[f]B. Hundhammer and T. Solomon. *J. Electroanal. Chem*. **157**, 19 (1983).
[g]Z. Samec, J. Langmaier, A. Trojánek. *J. Electroanal. Chem*. **409**, 1 (1996).
[h]J. Czapkiewicz and B. Czapkiewicz-Tutaj. *J. Chem. Soc., Faraday Trans. 1* **76**, 1663 (1980).
[i]M. H. Abraham and A. F. Danil de Namor. *J. Chem. Soc., Faraday Trans. 1* **72**, 955 (1976).
[j]A. Sabela, V. Mareček, Z. Samec, R. Fuoco. *Electrochim. Acta* **37**, 231 (1992).

Kinetic parameters of ion transfer have been evaluated mainly from impedance measurements by fitting the impedance data to the Randles-type equivalent circuit, cf. Fig. 10. Typical impedance plots (the imaginary vs. the real component of the complex impedance) are shown in Fig. 18 [117]. Diffusion coefficients and the apparent kinetic parameters for selected ions are listed in Table 3.

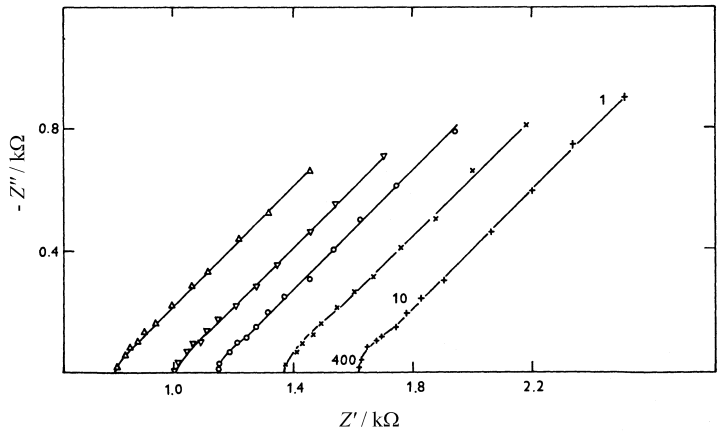

Fig. 18 Impedance plots for the water|nitrobenzene interface in the presence of picrate anion in both phases at temperatures of 278 K (+), 283 K (x), 293 K (o), 303 K (∇), and 313 K (Δ). Numbers on curves are frequencies in Hz. Reprinted with permission from [117]. © 1992 Elsevier Science.

Table 3 Ion diffusion coefficients D(w) and D(o) (in parentheses), and apparent kinetic parameters k_0^S and α for transfer of selected cations and anions across the water|nitrobenzene interface. Excerpted from [30].

Ion	10^6 D/cm^2 s^{-1}	10 k_0^s/cm s^{-1}	α
Cs^+	– (–)	0.66	0.56
Me_4N^+	10.6 (–)	0.90	0.50
	9.5 (3.7)	1.36	0.58
	9.5 (4.8)	1.20	–
Et_4N^+	7.8	1.50	0.55
	9.3 (4.0)	0.90	0.64
	9.3 (4.5)	1.10	–
	7.3 (–)	<10	–
	– (–)	2.20	–
Pr_4N^+	– (1.21)	0.47	0.44
	8.5 (3.4)	1.36	0.60
$Picrate^-$	6.1 (2.7)	0.83	0.56
	8.8 (–)	0.37	0.45
ClO_4^-	15.3 (6.7)	0.90	0.57
	14.9 (–)	1.08	0.53

3.7.2 Assisted ion transfer

When an ion association or complex formation, eq. 3, occurs in one or both liquid phases, the potential of the ion transfer shifts depending on the magnitude of the equilibrium constants of the coupled chemical reactions, eq. 4, cf. Fig. 16B. The measured potential difference can be used for the evaluation of the corresponding equilibrium constants, which are comparable with those derived from potentiometric measurement [118].

3.7.3 Photoinduced ion transfer

Irradiation of the ITIES by visible or UV light can give rise to a photocurrent, which is associated with the transfer of an ion in its excited state, or with the transfer of an ionic product of the photochemical reaction occurring in the solution bulk. Polarization measurements of the photoinduced ion transfer thus

extend the range of experimental approaches to photochemical processes, allowing us to investigate their mechanism on the one hand, and to study the specific effects of the electrical field on the other hand. Figure 19 shows photocurrent transient at a constant potential difference that is associated with the photochemical reactions of the tetraarylammonium ions [119].

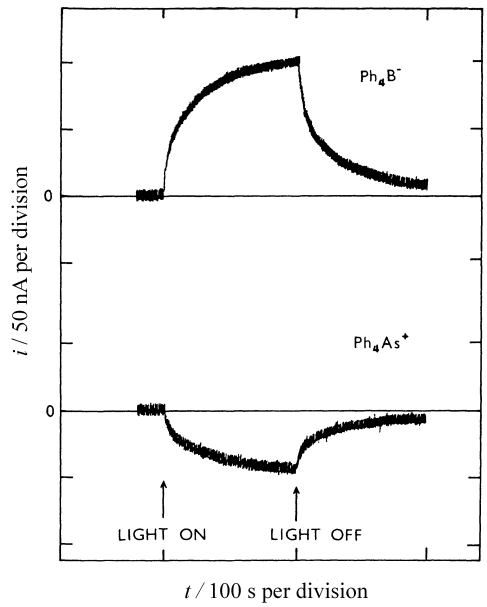

Fig. 19 Photocurrent transients for the interface between 0.01 mol dm^{-3} LiCl in water and 0.01 mol dm^{-3} tetrabutylammonium tetraphenylborate (TBATPB) or tetraphenylarsonium 7,8,9,10,11,12-hexabromohexahydro-1-carba-*closo*-dodecaborate (TPACBB) in 1,2-dichloroethane irradiated by monochromatic light at λ = 270 nm. Reprinted with permission from [119]. © 1990 Elsevier Science.

3.7.4 Simple electron transfer

Figure 20 shows a cyclic voltammogram of the electron transfer between the ferricenium$^+$/ferrocene redox couple in nitrobenzene and the hexacyanoferrate(III)/(II) redox couple in water [120]. Unlike the ion transfer, the electron-transfer processes at the ITIES are relatively slow and their kinetics can be evaluated with, e.g., slow cyclic voltammetry [121,122]. Nevertheless, most of the kinetic data have been obtained indirectly by SECM [111], see ref. [123] for review. A key issue is the effect of the standard electrochemical Gibbs energy of electron transfer $\Delta_w^o \tilde{G}_{el}^o$, eq. 43, on the rate constant of electron transfer. The latter was found to follow a parabolic dependence [124] in accordance with theoretical prediction [53], cf. eq. 43.

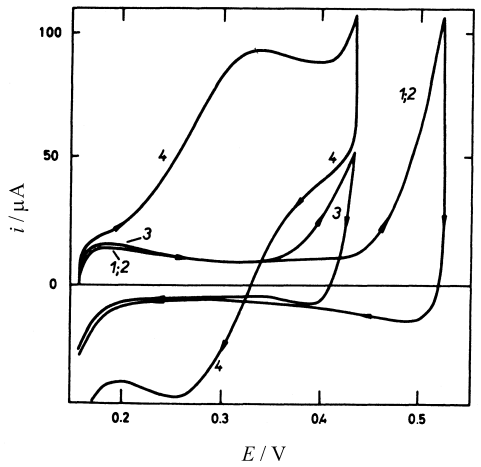

Fig. 20 Cyclic voltammograms of the water (W)|nitrobenzene (NB) interface in the presence of: (1) base electrolytes; (2) base electrolytes and ferrocene in NB; (3) base electrolyte and $Fe(CN)_6^{3-/4-}$ redox couple in W; (4) base electrolytes, $Fe(CN)_6^{3-/4-}$ in W and ferrocene in NB. Sweep rate 0.01 V s^{-1}. Reprinted with permission from [120]. © 1979 Elsevier Science.

3.7.5 Photoinduced electron transfer

Another approach to heterogeneous electron transfer relies on photoexcitable dye molecules adsorbed at the ITIES. As shown schematically in Fig. 21A [125], the general mechanism for a photoinduced electron transfer between a water-soluble sensitizer (S_W) and a redox quencher located in the organic

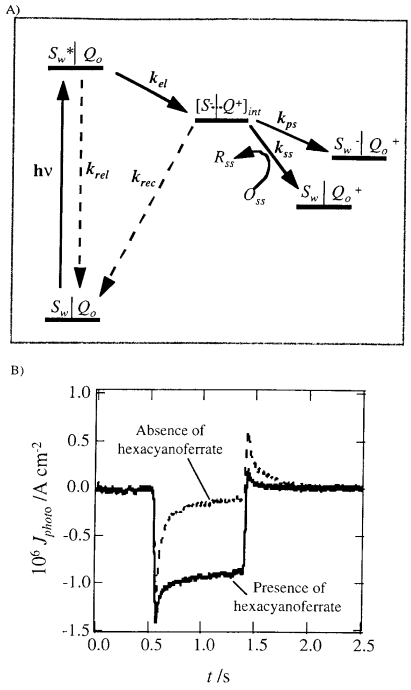

Fig. 21 (A) General mechanism for a photoinduced electron transfer between a sensitizer (S_W) in water and a quencher (Q_O) in the organic solvent phase. (B) Photocurrent transient associated with photoinduced electron transfer between a Zn porphyrin in water and TCNQ in 1,2-dichloroethane. Reprinted with permission from [125]. © 1999 Elsevier Science.

phase (Q_o) involves the competition between photoinduced electron transfer (k_{el}) and relaxation of the excited state (k_{rel}), as well as among product separation (k_{ps}), supersensitization (k_{ss}), and back electron transfer (k_{rec}). Figure 21B illustrates photocurrent responses associated with the heterogeneous quenching of the water-soluble Zn porphyrin by 7,7,8,8-tetracyanoquino-dimethane (TCNQ) in 1,2-dichloroethane in the presence and absence of hexacyanoferrate(II)/(III), which diminishes the back electron-transfer feature.

3.7.6 Structure of ITIES

Electrocapillary curves for ITIES that are measured in the absence of ionic or nonionic surfactants have a parabolic shape (Fig. 22). Analysis of surface tension data [126–128] suggests that the modified Verwey–Niessen model [128] represents a convenient description of the interfacial structure. According to this model, a layer of solvent molecules (the inner layer) separates two ionic space charge regions (diffuse double layers), the behavior of which can be described by the Gouy–Chapman theory [11,12]. An assumption of this model is that the potential difference $\Delta_o^w\phi$ can be expressed as the sum of three contributions [128]

$$\Delta_o^w\phi = \Delta_o^w\phi_{in} + \phi_2^o - \phi_2^w \tag{58}$$

where $\Delta_o^w\phi_{in}$, ϕ_2^o, and ϕ_2^w are the potential differences across the inner layer, and the space charge regions in the organic and the aqueous phases, respectively. The electrocapillary maximum was found at a potential (the potential of zero charge, PZC), which corresponds to $\Delta_o^w\phi \approx 0$, i.e., at the PZC where the inner-layer potential difference is rather small [127,128]. A similar result was obtained for the water-1,2-dichloroethane interface by the pendant-drop video-image [61], drop-time [129], and the streaming-jet electrode [130] techniques. On this basis, a method was proposed for measuring directly the Gibbs energy of ions by referring the values of the Galvani potential scale to the PZC [131]. Far from the PZC, the inner layer potential can reach several tens of millivolts [127]. Relatively small values of $\Delta_o^w\phi_{in}$ are consistent with the observation that the inner-layer thickness is less than unity when expressed as a number of monolayers of water. This is likely to be a consequence of interfacial solvent mixing and mixed solvation (mixed solvent layer) [132].

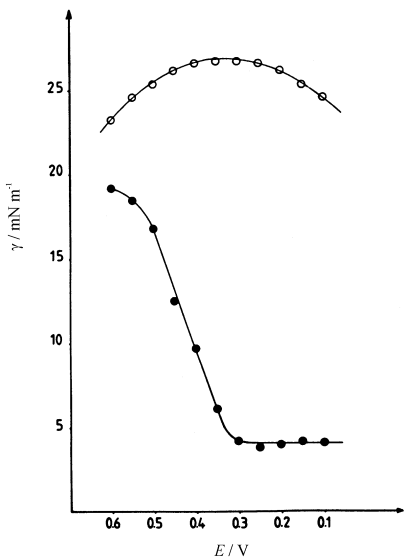

Fig. 22 Electrocapillary curves for (a) (○) the base electrolyte solutions; 0.02 M KCl in water and 1 mM tetrabutylammonium tetraphenylborate in 1,2-dichloroethane and (b) (●) after addition of 25 μM of phosphatidylcholine to the organic solvent phase. Adapted from [133].

Surface tension measurements have provided a wealth of data on the adsorption of ionic and non-ionic surfactants, as well as of compounds of biological significance, see refs. [25,27,30,33] for a review. Figure 22 [133] illustrates a remarkable drop in the surface tension of the water-1,2-dichloroethane interface in the presence of phosphatidylcholine, pointing to the formation of an adsorbed monolayer in a limited range of Galvani potential differences.

The differential capacity C of the electrical double layer at ITIES, eq. 54, has been studied mainly by impedance measurements [81]. The effects of the potential difference and the electrolyte concentration on the capacity, C, are illustrated in Fig. 23 [134]. The potential corresponding to the capacity minimum is usually found close to the PZC. The capacity data are consistent with the results of surface tension measurements [126], except for potentials far removed from the PZC [135].

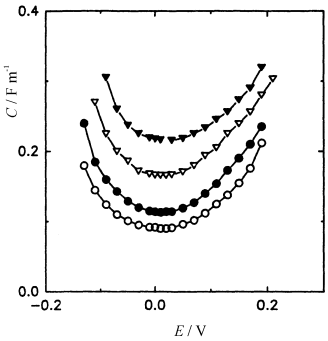

Fig. 23 Differential capacity C vs. the potential difference E across the water|nitrobenzene interface. Concentration (in mol dm^{-3}) of LiCl in water and tetrabutylammonium tetraphenylborate (TBATPB) in nitrobenzene: 0.01 (○), 0.02 (●), 0.05 (▽) and 0.1 (▲). Reprinted with permission from [134]. © 1995 Elsevier Science.

The technique of optical second harmonic generation has been shown to provide direct information about the surface coverage of ITIES by adsorbed dye molecules, cf. Fig. 24 [104].

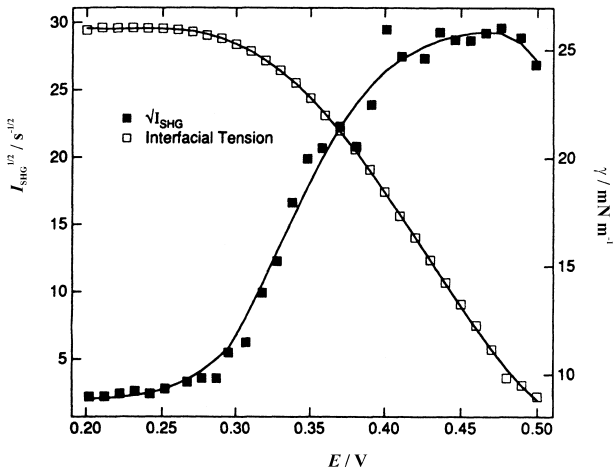

Fig. 24 Interfacial tension γ(□) and the square root of the SHG intensity $\sqrt{I_{SHG}}$ (■), as a function of the applied potential E for 20 μmol dm^{-3} 2-(*N*-octadecyl)aminonaphtalene-6-sulfonate, 50 mmol dm^{-3} KCl, and 25 mmol dm^{-3} Na_2HPO_4 in water (pH = 9) and 1 mmol dm^{-3} tetrabutylammonium tetraphenylborate in 1,2-dichloroethane. Reprinted with permission from [104]. © 1993 American Chemical Society.

Theoretical considerations about the molecular structure of the ITIES have been influenced by molecular dynamics simulations [136]. These indicate that the ITIES is molecularly sharp but very rough (Fig. 25).

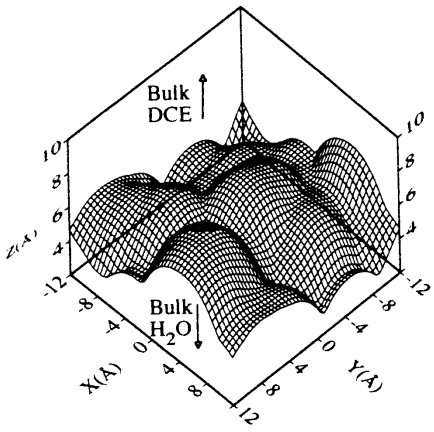

Fig. 25 A snapshot of the water surface in contact with 1,2-dichloroethane. Shown is the Conolly surface of the water's oxygen using a probe ball of radius 5 Å. The Gibbs surface is at $Z = 4$ Å. Reprinted with permission from [136]. © 1996 American Chemical Society.

4. PRACTICAL APPLICATIONS

4.1 Electroanalysis

Studies on polarized ITIES are relevant to the field of electroanalysis in two respects. First, they provide a fundamental knowledge, which allows us to explain the phenomena occurring at the membranes of ion-selective electrodes [137]. Second, ion transfer and assisted ion-transfer reactions at the ITIES, the rates of which are proportional to concentrations, can be used to design amperometric sensors [138]. Figure 26 illustrates the determination of alkali earth metal cations by differential pulse-stripping voltammetry at a hanging electrolyte drop electrode [139].

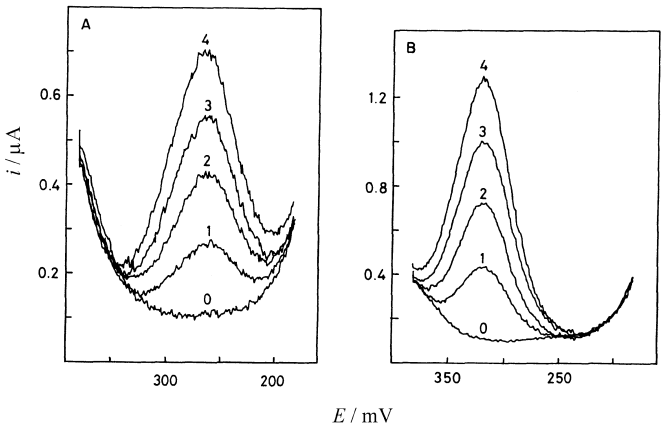

Fig. 26 Differential pulse-stripping voltammograms of (A) calcium and (B) barium ion transfer at the hanging electrolyte drop electrode. Concentrations (μmol dm^{-3}) of metal ion in the aqueous phase are indicated on the curves. Base electrolytes were 2.5 mmol dm^{-3} $MgCl_2$ in water and 5 mmol dm^{-3} tetrabutylammonium tetraphenylborate in nitrobenzene, with 1 mmol dm^{-3} macrocyclic polyether diamide ligand in the nitrobenzene. Reprinted with permission from [139]. © 1983 Elsevier Science.

4.2 Ion partition diagrams and drug delivery

Drugs are administrated mostly in their hydrophilic (usually protonated) forms. Their pharmacokinetics depends on several factors, of which one is drug lipophilicity. Since it is commonly accepted that the species crossing the biological membrane to reach the target site must be electrically neutral, drug lipophilicity is measured by the partition coefficient of the neutral drug form in a two-phase liquid system. From the electrochemical point of view, this approach is unsatisfactory, because the transfer of even highly lipophilic ions across the liquid and bilayer lipid membranes is possible. A more convenient approach that considers the partition of the neutral and the ionic drug forms, as well as the acid-base equilibria in both phases of the partition system has been proposed [140]. The approach is based on the construction of an ion partition diagram of the solute, which is analogous to Pourbaix's pH-potential diagrams widely used in the electrochemistry of corrosion. Essentially, the ion partition diagram defines the conditions of coexistence of various drug forms at different potential differences $\Delta_o^w\phi$ and different pH values. Three types of boundary lines are introduced. The first one follows from eq. 11 for a unity concentration ratio of an ion in the two liquid phases, i.e.,

$$\Delta_o^w\phi = \Delta_o^w\phi_i^{o'} \tag{59}$$

Equation 59 gives rise to a horizontal line in the $\Delta_o^w\phi$ vs. pH diagram. The second one follows from the apparent dissociation constant of the protonated base in the aqueous phase for a unity concentration ratio of the base and the conjugated acid, i.e.,

$$\mathrm{pH} = \mathrm{p}K_a' \tag{60}$$

which gives rise to a vertical line in the $\Delta_o^w\phi$ vs. pH diagram. The third one is a combination of the apparent dissociation constant of the protonated base in the organic phase and eq. 11 for the proton partition coefficient; the latter gives rise to an oblique line in the $\Delta_o^w\phi$ vs. pH diagram. The ion partition diagram of the anti-arrythmic drug quinidine including the mechanism of the transfer reactions resulting from the passage from one predominance domain to the other is shown in Fig. 27 [140].

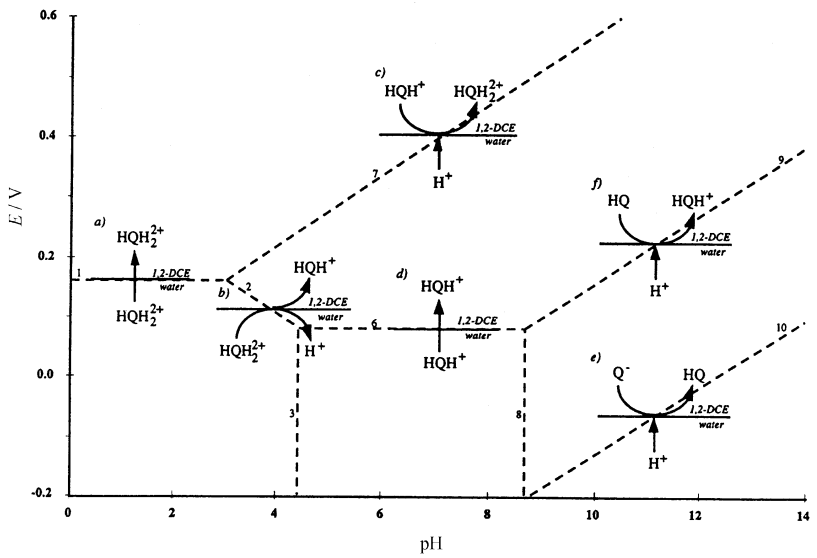

Fig. 27 Schematic transfer mechanisms of the various forms of quinidine (HQ) at the water|1,2-dichloroethane (DCE) interface. The following transfers are outlined: (a) simple HQH_2^{2+} transfer; (b) HQH_2^{2+} transfer by interfacial dissociation; (c) assisted proton transfer facilitated by HQH^+ (DCE); (d) simple HQH^+ transfer; (e) assisted proton transfer facilitated by Q^-; (f) assisted proton transfer facilitated by HQ (DCE). Reprinted with permission from [140]. © 1996 American Chemical Society.

4.3 Phase-transfer catalysis

Phase-transfer catalysis (PTC) has been utilized in organic synthesis to perform reactions in organic solvents when some of reactants are present in the aqueous phase, e.g., the substitution reaction involving alkylchlorides RCl,

$$RCl(o) + NaCN(w) = RCN(o) + NaCl \quad (61)$$

The rate of reaction (61) is negligible until a tetraalkylammonium chloride (A_4NCl) is added as a catalyst. It has been usually considered that the role of the catalyst is to physically transfer the reactant, as the ion pair $A_4N^+CN^-$, from the aqueous to the organic phase where the homogeneous chemical reaction can occur. While this may be the case in organic media of low dielectric permittivity, a different mechanism is more likely when the organic electrolytes can dissociate into ions. Essentially, the salt added as catalyst is capable of partitioning between the two liquid phases, thereby setting up a distribution potential, cf. eq. 22, that drives the ion (e.g., CN^-) or the electron to the target substance [20]. Therefore, polarization studies on the ITIES can help elucidate the mechanism of PTC, as well as provide a tool for the systematic search for suitable catalysts.

4.4 Electro-assisted extraction

Two-phase liquid systems or liquid membranes have found applications in various separation technologies. Liquid membranes have an advantage over traditional solvent extraction in that the volume of the organic phase can be considerably decreased and, hence, the costs associated with expensive solvents and ligands reduced. Electro-assisted extraction by the application of a potential difference across a polarizable liquid membrane appears to be a potential alternative [141].

4.5 Electrocatalysis

Charge-transfer processes comprising an intermediate or product adsorbed in the interfacial region σ, i.e., schematically

$$A(w) \rightarrow P(\sigma) \rightarrow B(o) \quad (62)$$

are of great practical interest. These processes include the deposition of a metal such as Cu at the ITIES [142], the preparation of colloidal metal particles with catalytic properties for homogeneous organic reactions [143], electropolymerization [144], and electron transfer through a ground [145] or excited state localized at the ITIES (photocatalysis) [146], cf. also Fig. 21.

ACKNOWLEDGMENTS

Financial support from Ministry of Education, Youth and Sports of the Czech Republic, Grant No. NONTAKT/ME 502, is gratefully acknowledged.

REFERENCES

1. W. Nernst. *Z. Phys. Chem.* **9**, 137 (1892).
2. R. Beutner. *Z. Elektrochem.* **19**, 319 (1913).
3. R. Beutner. *Z. Elektrochem.* **19**, 467 (1913).
4. R. Beutner. *Z. Elektrochem.* **24**, 94 (1918).
5. E. Baur. *Z. Elektrochem.* **19**, 590 (1913).
6. E. Baur. *Z. Elektrochem.* **32**, 547 (1926).
7. R. R. Dean. *Nature* **144**, 32 (1939).

8. K.-F. Bonhoeffer, M. Kahlweit, H. Strehlow. *Z. Elektrochem.* **57**, 614 (1953).
9. F. M. Karpfen and J. E. B. Randles. *Trans. Faraday Soc.* **49**, 823 (1953).
10. E. J. W. Verwey and K. F. Niessen. *Philos. Mag.* **28**, 435 (1939).
11. G. Gouy. *C. R. Acad. Sci.* **149**, 654 (1910).
12. D. L. Chapman. *Philos. Mag.* **25**, 475 (1913).
13. W. Nernst and E. H. Riesenfeld. *Ann. Phys.* **8**, 600 (1902).
14. J. Guastalla. *J. Chim. Phys.* **53**, 470 (1956).
15. J. Guastalla. *C. R. Acad. Sci. C* **276**, 17 (1973).
16. M. Blank. *J. Colloid Interface Sci.* **22**, 51 (1966).
17. C. Gavach, T. Mlodnicka, J. Guastalla. *C. R. Acad. Sci. C* **266**, 1196 (1968).
18. J. Koryta, M. Březina, P. Vanýsek. *J. Electroanal. Chem.* **75**, 211 (1977).
19. J. Koryta. *Electrochim. Acta* **24**, 293 (1979).
20. J. Koryta and P. Vanýsek. In *Advances in Electrochemistry and Electrochemical Engineering*, Vol. 12, H. Gerischer and C. W. Tobias (Eds.), p. 113, Wiley-Interscience, New York (1981).
21. J. Koryta. *Ion-Select. Electrode Rev.* **5**, 131 (1983).
22. J. Koryta. *Electrochim. Acta* **29**, 445 (1984).
23. H. H. Girault. *Electrochim. Acta* **32**, 383 (1987).
24. J. Koryta. *Electrochim. Acta* **33**, 189 (1988).
25. Z. Samec. *Chem. Rev*. **88**, 617 (1988).
26. V. Mareček, Z. Samec, J. Koryta. *Adv. Colloid Interface Sci.* **29**, 1 (1988).
27. H. H. Girault and D. J. Schiffrin. In *Electroanalytical Chemistry*, Vol. 15, A. J. Bard (Ed.), p. 1, Marcel Dekker, New York (1989).
28. M. Senda, T. Kakiuchi, T. Osakai. *Electrochim. Acta* **36**, 253 (1991).
29. H. H. Girault. In *Modern Aspects of Electrochemistry*, Vol. 25, R. E. White, B. E. Conway, J. O'M. Bockris (Eds.), p. 1, Plenum, New York (1993).
30. Z. Samec and T. Kakiuchi. In *Advances in Electrochemistry and Electrochemical Science*, Vol. 4, H. Gerischer and C. W. Tobias (Eds.), p. 297, VCH, Weinheim (1995).
31. P. Vanýsek. *Electrochemistry at Liquid–Liquid Interfaces*, Lecture Notes in Chemistry, Vol. 39, Springer, Berlin (1985).
32. V. E. Kazarinov (Ed.). *The Interface Structure and Electrochemical Processes at the Boundary Between Two Immiscible Liquids*, Springer, Berlin (1987).
33. A. G. Volkov and D. W. Deamer (Eds.). *Liquid–Liquid Interfaces: Theory and Methods*, CRC Press, Boca Raton (1996).
34. A. G. Volkov, D. W. Deamer, D. L. Tanelian, V. S. Markin (Eds.). *Liquid Interfaces in Chemistry and Biology*, John Wiley, New York (1998).
35. Z. Samec. *J. Electroanal. Chem.* **99**, 197 (1979).
36. Z. Samec, V. Mareček, J. Weber, D. Homolka. *J. Electroanal. Chem.* **126**, 105 (1981).
37. L. Q. Hung. *J. Electroanal. Chem.* **115**, 159 (1980).
38. L. Q. Hung. *J. Electroanal. Chem.* **149**, 1 (1983).
39. T. Kakiuchi. *Anal. Chem.* **68**, 3658 (1996).
40. T. Kakiuchi. *Electrochim. Acta* **40**, 2999 (1995).
41. A. J. Parker. *Chem. Rev.* **69**, 1 (1969).
42. M. H. Abraham. *J. Chem. Soc. B* 299 (1971).
43. H. H. Girault and D. J. Schiffrin. *J. Electroanal. Chem.* **195**, 213 (1985).
44. Z. Samec, Yu. I. Kharkats, Yu. Ya. Gurevich. *J. Electroanal. Chem.* **204**, 257 (1986).
45. T. Kakiuchi. *J. Electroanal. Chem.* **322**, 55 (1992).
46. W. Schmickler. *J. Electroanal. Chem.* **426**, 5 (1997).
47. R. A. Marcus. *J. Chem. Phys*. **113**, 1618 (2000).
48. I. Benjamin. *J. Chem. Phys*. **96**, 577 (1992).
49. M. Senda. *Electrochim. Acta* **40**, 2993 (1995).

50. K. Kontturi, J. A. Manzanares, L. Murtomäki. *Electrochim. Acta* **40**, 2979 (1995).
51. Yu. I. Kharkats. *Sov. Electrochem.* **12**, 1257 (1986).
52. H. H. Girault and D. J. Schiffrin. *J. Electroanal. Chem.* **244**, 15 (1988).
53. R. A. Marcus. *J. Phys. Chem.* **94**, 1050 (1990).
54. V. G. Levich. *Adv. Electrochem. Electrochem. Eng.* **4**, 249 (1966).
55. R. A. Marcus. *J. Chem. Phys.* **43**, 679 (1965).
56. Z. Koczorowski. In *The Interface Structure and Electrochemical Processes at the Boundary Between Two Immiscible Liquids*, V. E. Kazarinov (Ed.), p. 77, Springer, Berlin (1987).
57. D. J. Clarke, D. J. Schiffrin, M. C. Wiles. *Electrochim. Acta* **34**, 767 (1989).
58. Z. Koczorowski and I. Zagórska. *J. Electroanal. Chem.* **159**, 183 (1983).
59. A. W. Adamson. *Physical Chemistry of Surfaces*, 5th ed., p. 122, John Wiley, New York (1990).
60. T. Kakiuchi and M. Senda. *Bull. Chem. Soc. Jpn.* **56**, 2912 (1983).
61. H. H. Girault and D. J. Schiffrin. *J. Electroanal. Chem.* **170**, 127 (1984).
62. G. Lippmann. *Ann. Chim. Phys.* **5**, 794 (1875).
63. C. Gavach and F. Henry. *J. Electroanal. Chem.* **54**, 361 (1974).
64. Z. Samec, V. Mareček, J. Weber. *J. Electroanal. Chem.* **100**, 841 (1979).
65. V. Mareček and Z. Samec. *Anal. Lett.* **14**, 1241 (1981).
66. T. Osakai, T. Kakutani, M. Senda. *Bull. Chem. Soc. Jpn.* **57**, 370 (1984).
67. O. R. Melroy, W. E. Bronner, R. P. Buck. *J. Electrochem. Soc.* **130**, 373 (1983).
68. B. Hundhammer, S. K. Dhawan, A. Bekele, H. J. Sedlitz. *J. Electroanal. Chem.* **217**, 253 (1987).
69. T. Osakai, T. Kakutani, M. Senda. *Bunseki Kagaku* **33**, E371 (1984).
70. H. H. Girault and D. J. Schiffrin. *J. Electroanal. Chem.* **137**, 207 (1982).
71. J. Koryta, M. Březina, P. Vanýsek. *J. Electroanal. Chem.* **67**, 263 (1976).
72. Z. Samec, V. Mareček, J. Weber, D. Homolka. *J. Electroanal. Chem.* **99**, 385 (1979).
73. T. Ohkouchi, T. Kakutani, T. Osakai, M. Senda. *Rev. Polarography (Kyoto)* **31**, 123 (1985).
74. J. A. Campbell and H. H. Girault. *J. Electroanal. Chem.* **266**, 465 (1989).
75. O. Shirai, S. Kihara, M. Suzuki, K. Ogura, M. Matsui. *Anal. Sci. (Suppl.)* **7**, 607 (1991).
76. H. C. Visser, D. N. Reinhoudt, F. de Jong. *Chem. Soc. Rev*. 75 (1994).
77. C. Beriet and H. H. Girault. *J. Electroanal. Chem.* **444**, 219 (1998).
78. A. Craggs, L. Keil, G. J. Moody, J. D. R. Thomas. *Talanta* **22**, 907 (1975).
79. W. J. Albery, J. F. Burke, E. B. Leffler, J. D. Hadgraft. *J. Chem. Soc., Faraday Trans. 1* **72**, 1618 (1976).
80. J. A. Manzanares, R. Lahtinen, B. Quinn, K. Kontturi, D. J. Schiffrin. *Electrochim. Acta* **44**, 59 (1998).
81. Z. Samec, V. Mareček, D. Homolka. *J. Electroanal. Chem.* **126**, 121 (1981).
82. V. Mareček and Z. Samec. *J. Electroanal. Chem.* **149**, 185 (1983).
83. Y. Shao and H. H. Girault. *J. Electroanal. Chem.* **282**, 59 (1990).
84. T. Kakutani, T. Osakai, M. Senda. *Bull. Chem. Soc. Jpn.* **56**, 991 (1983).
85. Z. Samec. *J. Electroanal. Chem.* **111**, 211 (1980).
86. C. Gavach, P. Seta, F. Henry. *Bioelectrochem. Bioenerg.* **1**, 329 (1974).
87. S. Kihara, Z. Yoshida, T. Fujinaga. *Bunseki Kagaku* **31**, 297 (1982).
88. V. Mareček, M. Grätzel, A. Pungor, J. Janata. *J. Electroanal. Chem.* **266**, 239 (1989).
89. R. M. Allen, K. Kontturi, L. Murtomaki, D. E. Williams. *J. Electroanal. Chem.* **483**, 57 (2000).
90. Z. Samec. *J. Electroanal. Chem.* **103**, 1 (1979).
91. A. A. Stewart, J. A. Campbell, H. H. Girault, M. Eddowes. *Ber. Bunsen-Ges. Phys. Chem.* **94**, 83 (1990).
92. H. Matsuda, Y. Yamada, K. Kanamori, Y. Kudo, Y. Takeda. *Bull. Chem. Soc. Jpn.* **64**, 1497 (1991).
93. D. Homolka, K. Holub, V. Mareček. *J. Electroanal. Chem.* **138**, 29 (1982).
94. T. Kakiuchi and M. Senda. *J. Electroanal. Chem.* **300**, 431 (1991).

95. F. Reymond, P.-A. Carrupt, H. H. Girault. *J. Electroanal. Chem.* **449**, 49 (1998).
96. F. Reymond, G. Lagger, P.-A. Carrupt, H. H. Girault. *J. Electroanal. Chem.* **451**, 59 (1998).
97. L. Tomaszewski, F. Reymond, P.-F. Brevet, H. H. Girault. *J. Electroanal. Chem.* **483**, 135 (2000).
98. T. Kakiuchi. *Electrochim. Acta* **44**, 171 (1998).
99. Z. Samec, A. Trojánek, J. Langamier, E. Samcová. *J. Electroanal. Chem.* **481**, 1 (2000).
100. T. Kakiuchi, Y. Takasu, M. Senda. *Anal. Chem.* **64**, 3096 (1992).
101. Z. Ding, R. G. Wellington, P.-F. Brevet, H. H. Girault. *J. Electroanal. Chem.* **420**, 35 (1997).
102. T. Kakiuchi and Y. Takasu. *Anal. Chem.* **66**, 1853 (1994).
103. Z. Ding, F. Reymond, P. Baumgartner, D. J. Fermín, P.-F. Brevet, P.-A. Carrupt, H. H. Girault. *Electrochim. Acta* **44**, 3 (1998).
104. D. A. Higgins and R. M. Corn. *J. Phys. Chem.* **97**, 489 (1993).
105. Z. Zhang, I. Tsuyumoto, S. Takahashi, T. Kitamori, T. Sawada. *J. Phys. Chem. A* **101**, 4163 (1997).
106. A. Trojánek, P. Krtil, Z. Samec. *Electrochem. Commun*. **3**, 613 (2001).
107. J. Strutwolf, A. L. Barker, M. Gonsalves, D. J. Caruana, P. R. Unvin, D. E. Williams, J. R. P. Webster. *J. Electroanal. Chem.* **483**, 163 (2000).
108. R. A. W. Dryfe, R. D. Webster, B. A. Coles, R. G. Compton. *Chem. Commun.* 779 (1992).
109. R. D. Webster and D. Beaglehole. *Phys. Chem. Chem. Phys.* **2**, 5660 (2000).
110. H. H. J. Girault, D. J. Schiffrin, B. D. V. Smith. *J. Electroanal. Chem.* **137**, 207 (1982).
111. C. Wei, A. J. Bard, M. V. Mirkin. *J. Phys. Chem.* **99**, 16033 (1995).
112. C. J. Slevin and P. R. Unwin. *Langmuir* **13**, 4799 (1997).
113. Z. Samec, A. Trojánek, J. Langamier. *J. Electroanal. Chem.* **444**, 1 (1998).
114. O. Valent, J. Koryta, M. Panoch. *J. Electroanal. Chem.* **226**, 21 (1987).
115. G. Geblewicz, A. K. Kontturi, D. J. Schiffrin. *J. Electroanal. Chem.* **217**, 261 (1987).
116. O. Dvořák, V. Mareček, Z. Samec. *J. Electroanal. Chem.* **300**, 407 (1991).
117. T. Wandlowski, V. Mareček, Z. Samec, R. Fuoco. *J. Electroanal. Chem.* **331**, 765 (1992).
118. Z. Samec, D. Homolka, V. Mareček. *J. Electroanal. Chem.* **135**, 265 (1982).
119. Z. Samec, A. R. Brown, L. J. Yellowlees, H. H. Girault. *J. Electroanal. Chem.* **288**, 245 (1990).
120. Z. Samec, V. Mareček, J. Weber. *J. Electroanal. Chem.* **96**, 245 (1979).
121. Z. Samec, V. Mareček, J. Weber, D. Homolka. *J. Electroanal. Chem.* **126**, 105 (1981).
122. G. Geblewicz and D. J. Schiffrin. *J. Electroanal. Chem.* **244**, 27 (1988).
123. S. Amemiya, Z. Ding, J. Zhou, A. J. Bard. *J. Electroanal. Chem.* **483**, 7 (2000).
124. A. L. Barker, P. R. Unwin, S. Amemiya, J. Zhou, A. J. Bard. *J. Phys. Chem. B* **103**, 7260 (1999).
125. D. J. Fermin, H. Doung, Z. Ding, P.-F. Brevet, H. Girault. *Electrochem. Commun.* **1**, 29 (1999).
126. T. Kakiuchi and M. Senda. *Bull. Chem. Soc. Jpn.* **56**, 1322 (1983).
127. T. Kakiuchi and M. Senda. *Bull. Chem. Soc. Jpn.* **56**, 1753 (1983).
128. C. Gavach, F. Henry, B. d'Epenoux. *J. Electroanal. Chem.* **83**, 225 (1977).
129. Z. Samec, V. Mareček, K. Holub, S. Račinský, P. Hájková. *J. Electroanal. Chem.* **225**, 65 (1987).
130. H. H. J. Girault and D. J. Schiffrin. *J. Electroanal. Chem.* **195**, 213 (1985).
131. H. H. Girault and D. J. Schiffrin. *Electrochim. Acta* **31**, 1341 (1986).
132. H. H. Girault and D. J. Schiffrin. *J. Electroanal. Chem.* **150**, 43 (1983).
133. H. H. Girault and D. J. Schiffrin. *J. Electroanal. Chem.* **179**, 277 (1984).
134. T. Wandlowski, K. Holub, V. Mareček, Z. Samec. *Electrochim. Acta* **40**, 2887 (1995).
135. Z. Samec, A. Lhotský, H. Jänchenová. *J. Electroanal. Chem.* **483**, 47 (2000).
136. I. Benjamin. *Chem. Rev.* **96**, 1449 (1996).
137. T. Kakiuchi and M. Senda. *Bull. Chem. Soc. Jpn.* **57**, 1801 (1984).
138. V. Mareček and Z. Samec. *Anal. Lett.* **14(B15)**, 1241 (1981).
139. V. Mareček and Z. Samec. *Anal. Chim. Acta* **151**, 265 (1983).
140. F. Reymond, G. Steyaert, P.-A. Carrupt, B. Testa, H. Girault. *J. Am. Chem. Soc.* **118**, 11951 (1996).

141. O. Shirai, S. Kihara, Y. Yoshida, M. Matsui. *J. Electroanal. Chem.* **389**, 61 (1995).
142. M. Guinazzi, G. Silvestri, G. Serravalle. *J. Chem. Soc., Chem. Commun.* 200 (1975).
143. Y. Cheng and D. J. Schiffrin. *J. Chem. Soc., Faraday Trans.* **92**, 3865 (1996).
144. V. J. Cunnane and U. Evans. *Chem. Commun.* 2163 (1998).
145. Y. Cheng and D. J. Schiffrin. *J. Chem. Soc., Faraday Trans.* **90**, 2517 (1994).
146. D. J. Fermin, Z. Ding, H. D. Doung. P.-F. Brevet, H. H. Girault. *Chem. Commun.* 1125 (1998).
147. Z. Samec, J. Langamier, A. Trojánek. *J. Electroanal. Chem.* **409**, 1 (1996).